Contents

N. Jerram PhD thesis 1995
DAMTP University of Cambridge
The effect of a group of obstacles on flow and dispersion over a surface

Chapter 3

Analytical models for turbulent canopy flows

3.1 Introduction

The interesting flows that can be modelled using the concept of distributed force—forests, urban areas, etc.—are generally characterised by large enough Reynolds numbers for the flow to be fully turbulent. Given such practical importance, the remaining chapters of this thesis are concerned specifically with *turbulent* flow and dispersion through a distributed force.

Turbulent flow field modelling in this thesis has two main objectives. Firstly we aim to produce practical analytical models for the detailed perturbation velocities and shear stresses within and above a region of distributed resistance. Such models are developed by the following analyses in this chapter, and have been incorporated into a working computer software package. The input to this computer package is a description of the incident wind and of the distributed resistance; the output is a two-dimensional array of perturbation flow quantities. In chapter 4 these models are used to simulate a number of experiments on flow through a group of obstacles and the simulation results are compared against the experimental data.

Secondly we aim to produce "equivalent" parameterisations, that usefully describe

broad aspects of the calculated flow fields in an accessible way. The most important of such parameterisations calculates effective roughness parameters—displacement height, roughness height and friction velocity—for the flow above a region of resistance that varies slowly in the streamwise direction. Chapter 5 derives two equivalent parameterisations from the detailed flow field results of chapter 3 and indicates the regions of the flow where these parameterisations are valid.

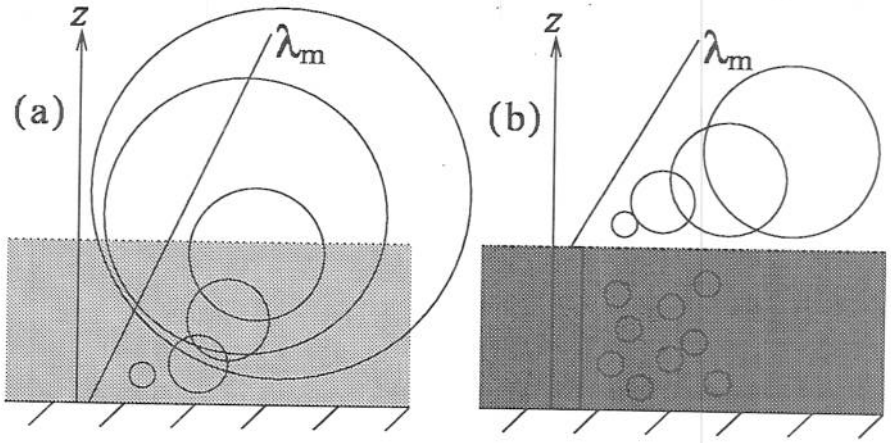

Figure 3.1: The two turbulent mixing length models used here. (a) The "standard" mixing length (SML) model. (b) The "displaced" mixing length (DML) model.

A turbulent analysis requires a model for the turbulent stresses. If a standard model such as mixing length or K–ϵ is to be used, new effects particular to distributed force flow or to the underlying canopy flow must be taken into account. For example, Svensson & Häggkvist (1990) and Savill & Solberg (1994) add terms to the K–ϵ turbulent kinetic energy (TKE) equation to represent the shear production of TKE in obstacle boundary layers.

In this chapter we use two variants of the mixing length model. The "standard" mixing length (SML) model (figure 3.1a) assumes that the mean flow perturbations due to a distributed force are too weak to alter the turbulence structure of the incident boundary layer flow. Hence the mixing length λ_m is proportional to height above the

ground. In the "displaced" mixing length (DML) model (figure 3.1b), the flow domain is divided into two. A constant mixing length within the canopy models intense small scale turbulence due to the eddies shed from individual obstacles, while a linear mixing length above, with a non-zero displacement height, models the blocking effect on turbulent eddies of a strong shear layer such as might be produced at the rooftop level of a group of obstacles. Thus the DML model assumes that individual obstacles and large scale mean flow changes significantly alter the turbulence structure within and above the obstacle canopy. The ideas behind these two contrasting turbulence models are further discussed in §3.2 and §3.8. The sensitivity of our results to turbulence modelling will be assessed by comparing results from these two models with each other and with numerical simulations using the K–ϵ closure.

For the SML turbulence model, the method of analysis of the perturbation flow field follows that of Jackson & Hunt (1975), Sykes (1980), Hunt *et al.* (1988a) and Belcher *et al.* (1990), developed by these authors in investigations of turbulent boundary layer flow over changes in ground elevation and surface roughness. The key points of this method are that

- the analysis is linear: we specify the form of the incident velocity upstream of any distributed force and assume that any perturbations from this incident profile are small;
- the flow domain is divided into dynamically distinct layers (described in §3.3): turbulent shear stresses usually affect the mean flow perturbations only within a thin layer near the ground (Townsend 1965);
- linear perturbations are calculated separately in each layer and then matched with each other using the method of matched asymptotic expansions.

Rapidly varying force distributions, however, can make turbulent shear stresses significant outside the thin stress layer near the ground (§3.4). This feature is specific to the distributed force problem, because a distributed force extends vertically into the flow domain, whereas the previously studied elevation and roughness changes are

surface perturbations. Hence separate analyses are presented for slowly varying (§3.5) and rapidly varying (§3.6) force distributions. Sample results for the SML analysis are presented in §3.7.

For the DML turbulence model (§3.8), the upper part of the flow, where mixing length increases linearly with height, is calculated using the same asymptotic method but with extensions to allow for a non-zero displacement height. The lower part of the flow, where mixing length is uniform, is calculated using the laminar viscous analysis of §2.9.

The chapter concludes in §3.9 by evaluating the sensitivity of the key features of the calculated flow fields to the turbulence model.

3.2 The SML turbulent stress model

As in the laminar analyses of chapter 2, the region of distributed force is characterised by horizontal and vertical extents L^* and H^*. The incident boundary layer flow is understood to be developing slowly only on time scales longer than the time L^*/U_o^* for flow to pass through the region of resistance, and the distributed force is taken to lie within the lower 20% of the total boundary layer depth. Hence the incident mean velocity profile is logarithmic (*e.g.* Panofsky & Dutton 1984, chapter 6) and characterised by friction velocity u_* and roughness height z_o^*:

$$U^*(z^*) = \frac{u_*}{\kappa} \ln \frac{z^*}{z_o^*}, \tag{3.1}$$

where $\kappa \approx 0.41$ is von Karman's constant. Hence the mixing length model for the undisturbed boundary layer shows that turbulent shear stress in the incident flow is uniform:

$$T^* = \rho u_*^2. \tag{3.2}$$

Throughout the analysis, capital letters denote incident flow quantities and lowercase letters perturbation quantities.

Following Townsend (1965), turbulent stress perturbations are modelled by the

equation

$$\tau^* = 2\rho u_* \kappa z^* \frac{\partial u^*}{\partial z^*}, \tag{3.3}$$

in which κz^* is the SML model turbulent mixing length. Equation (3.3) is the linear perturbation of the mixing length model for total shear stress, namely

$$\hat{\tau}^* = \rho \kappa^2 z^{*2} \frac{\partial \hat{u}^*}{\partial z^*} \left| \frac{\partial \hat{u}^*}{\partial z^*} \right|. \tag{3.4}$$

The factor of two in (3.3) arises because (3.4) makes total shear stress $\hat{\tau}^*$ quadratic in the total streamwise velocity gradient $\partial \hat{u}^*/\partial z^*$.

The normal stress perturbations τ^*_{11} and τ^*_{33} are far less important dynamically than the shear stress τ^*_{13} (also written here as τ^*). The flow within the thin layer where turbulent stress perturbations are non-negligible is largely determined by the balance of streamwise momentum, which is influenced by the *vertical* gradient of τ^*_{13} and the *streamwise* gradient of τ^*_{11}. Given that τ^*_{11} and τ^*_{13} are of similar order (as established by numerous experiments, *e.g.* Laufer 1955), the thinness of the turbulent stress layer makes $\partial \tau^*_{11}/\partial x^*$ negligible in comparison with $\partial \tau^*_{13}/\partial z^*$. In terms of the ratio ϵ between vertical and streamwise length scales in this layer, the normal stress τ^*_{11} makes only an $O(\epsilon^2)$ correction to the flow.

The vertical normal stress τ^*_{33} affects streamwise momentum transfer only indirectly, as it gives rise to a pressure variation across the thin layer at $O(\epsilon)$ and hence to an $O(\epsilon)$ correction to the streamwise velocity perturbation. This is omitted in the analysis below, even though corrections of similar order are included, because it exhibits no new interesting physics and because the analysis clearly indicates how an arbitrary number of further such corrections could be incorporated if so desired.

Thus closure models for τ^*_{11} and τ^*_{33} are not used in the following analysis. If models were required, for example to calculate further corrections to the asymptotic results below, then observations would suggest proportionality: $\tau^*_{11} = -\alpha \tau^*_{13}$ and $\tau^*_{33} = -\beta \tau^*_{13}$. Appropriate values for α and β, measured in the laboratory and in the atmosphere, are given by Townsend (1976, Table 5.2).

All quantities in the following analysis will be non-dimensionalised using the length L^*, advective velocity scale $U^*_o \equiv U^*(H^*)$ and fluid density ρ, with the exception of

turbulent shear stresses which scale on u_*^2 and so are conveniently non-dimensionalised by the incident shear stress ρu_*^2. Dimensional quantities are marked with an asterisk.

3.3 Asymptotic flow structure

3.3.1 The domain of importance of turbulent stresses

Implicit in the derivation of the mixing length model (3.3) is the idea that turbulent eddies are in a state of "local equilibrium" (Townsend 1961), such that there is enough time for turbulent eddies to move and transfer momentum before the mean flow has changed much. If, however, the mean flow changes too rapidly, eddies are distorted by the mean flow changes before there is time to establish the local equilibrium. The analogy with molecular diffusion then breaks down. In the limit of very rapidly changing mean flow, rapid distortion theory (RDT) can be used to model the turbulence. Following Britter *et al.* (1981) and Belcher *et al.* (1993), the height l^* of an inner region within which (3.4) applies is established by comparing time scales for turbulent eddy diffusion and for distortion of the mean flow.

Consider boundary layer flow past an obstacle of length L^*. The time taken for a fluid particle or an eddy to be advected past the obstacle at a height z^* is

$$t_a^* \approx L^*/U^*(z^*). \tag{3.5}$$

t_a^* decreases with height because the wind speed increases. The mean flow is distorted most somewhere near the obstacle, while far upstream and downstream the perturbations tend to zero. Hence t_a^* is also the characteristic time scale for mean flow distortion.

A turbulent equilibrium time t_e^* is determined by the turbulent length scale, which according to the mixing length theory is the height above the ground, and the characteristic velocity fluctuation u_*. The equilibrium time scale is therefore

$$t_e^* \approx z^*/u_*. \tag{3.6}$$

t_e^* increases with height as the typical eddy size increases, because more time is required to mix momentum over greater distances.

The two time scales t_a^* and t_e^* are of similar order at a height l^* defined implicitly by

$$\frac{L^*}{U^*(l^*)} \approx \frac{l^*}{u_*} \Rightarrow l^* \ln \frac{l^*}{z_o^*} \approx \kappa L^*. \tag{3.7}$$

In the region $z^* < l^*$ where the equilibrium time t_e^* is less than the advection time, the local equilibrium hypothesis is appropriate and the perturbation turbulence closure (3.3) can be used. For $z^* \gg l^*$, $t_e^* \gg t_a^*$ and so turbulence is governed by RDT. RDT implies that perturbation turbulent stresses are $O(\epsilon^2)$, where ϵ is the ratio of turbulent velocity u_* to characteristic advection velocity U_o^*. It follows that these rapidly distorted eddies have no effect on the leading order mean flow perturbations.

Thus consideration of these two time scales divides the flow domain into two regions at an approximate height l^*. In the inner region, *i.e.* $z^* < l^*$, turbulent stress perturbations are significant and can be modelled by the mixing length closure (3.3). In the outer region, $z^* > l^*$, turbulent stresses do not affect the mean flow perturbations at leading order, indicating that the outer region flow perturbations are effectively controlled by inertia gradients and pressure forces.

Belcher *et al.* (1993) have shown that this layered turbulence model is significantly more accurate than using a mixing length model throughout the flow domain when applied to the calculation of pressure drag on a low hill: the results of their linear asymptotic analysis are comparable with those of numerical simulations using a second-order turbulence closure. If an SML closure is used incorrectly outside the inner region, turbulent stress appears to affect the mean flow perturbations at $O(\epsilon)$, where ϵ is the ratio of turbulent friction velocity to the advective velocity scale. Belcher *et al.* used rapid distortion theory outside the inner region to show that turbulent stress in fact affects mean flow perturbations only at $O(\epsilon^2)$.

3.3.2 The use of Fourier analysis

Following Lighthill (1957) and many others, the application of Fourier analysis to the linearised distributed force problem allows arbitrary force distributions to be treated by the Fourier synthesis of a set of harmonic distributions. The inconvenience of inverse Fourier transformation at the end of the analysis is far outweighed by the simplification that results from reducing partial differential equations in two or three independent variables to ordinary differential equations in just one vertical coordinate.

Moreover, in the distributed force problem the reponse of the incident flow is quite different, depending on whether the force distribution varies rapidly or slowly in the streamwise direction, *i.e.* according to the ratio between streamwise variation length scale and force distribution height. Fourier analysis provides a formal method for separating out these differently behaving components of an arbitrary force distribution. This is an important extra consideration for the distributed force and roughness change problems because the imposed flow disturbance can include a wide spectrum of streamwise wavenumbers (consider the step change in roughness).

In a Fourier analysis, it is appropriate to calculate the height l^* separately for each Fourier component of the force distribution, taking the Fourier wavelength $2\pi/k^*$ as the horizontal length scale for advection. Thus, from (3.7), at each wavenumber k^* we define $l^*(k^*)$ implicitly by

$$k^* l^* \ln \frac{l^*}{z_o^*} \approx 2\pi\kappa. \tag{3.8}$$

This wavenumber dependent scaling leads naturally to the physical picture described in §1.5. The impact and exit regions of the flow correspond to short wavelength components of the force distribution. For these Fourier components l^* is small compared to the height of the force distribution and most of the perturbation flow will be inviscid as the physical arguments of §1.5 suggest. By contrast, in the array interior and far wake regions, which correspond to long wavelength components, l^* is large and well above the top of the force distribution; hence turbulent stresses are crucial to the dynamics of these regions.

To fix the value of l^* the right hand side of (3.8) is chosen to be 1. Note that

this choice is slightly different to that made by Hunt *et al.* (1988a) and Belcher *et al.* (1990) and is made here for notational convenience. Since l^* is interpreted as an order of magnitude estimate for the transition height between inner and outer regions, the choice of this $O(1)$ constant in no way affects the results. Thus l^* is defined implicitly by

$$k^* l^* \ln \frac{l^*}{z_o^*} = 1. \tag{3.9}$$

At very small wavenumbers (3.9) gives the inner region height l^* increasing without limit. In practice l^* must be limited by that fraction of the *incident* boundary layer depth in which there is local equilibrium, typically about one fifth of the total boundary layer depth. Denoting this limiting height by δ^*, there is a critical wavenumber k_c^* below which l^* as defined by (3.9) would exceed δ^*. k_c^* is given by

$$k_c^* = \left(\delta^* \ln \frac{\delta^*}{z_o^*} \right)^{-1}. \tag{3.10}$$

To estimate a typical value for k_c^* in the atmospheric boundary layer, we take $\delta^* = 200\text{m}$ and $z_o^* = 0.1\text{m}$, giving $k_c^* = 6.6 \times 10^{-4}\text{m}^{-1}$ or a critical horizontal scale of about 10km. This restriction is always significant for the smallest woods and villages as well as the largest cities and forests because, assuming that all of a force distribution acts in the same direction, the zero wavenumber Fourier component is larger in magnitude than any non-zero wavenumber component:

$$|f(k)| = \left| \int_{-\infty}^{\infty} f(x) e^{-ikx}\, dx \right| \leq \int_{-\infty}^{\infty} |f(x)|\, dx = |f(0)|. \tag{3.11}$$

In a numerical implementation of the results of the present analysis, (3.9) is modified to give

$$l^* \equiv \delta^* \tanh \frac{l_1^*}{\delta^*}, \quad \text{where} \quad k^* l_1^* \ln \frac{l_1^*}{z_o^*} = 1. \tag{3.12}$$

The value of l^* given by (3.12) differs negligibly from that of (3.9) when $k^* \gg k_c^*$, so the physical reasoning behind (3.9) is preserved until l^* approaches δ^*; then the modified definition (3.12) ensures that the stronger constraint $l^* \leq \delta^*$ is obeyed.

3.3.3 The asymptotic small parameter ϵ

The small parameter ϵ of the analysis is defined as the ratio between turbulent velocity scale u_* and advective velocity scale U_o^*:

$$\epsilon \equiv \frac{u_*}{\kappa U_o^*}. \tag{3.13}$$

Non-dimensionalisation of the advective velocity scale, $U_o^* = U^*(H^*)$, gives the relation

$$\epsilon \ln \frac{H}{z_o} = 1. \tag{3.14}$$

This is perhaps a more useful definition of ϵ since it relates the small parameter directly to the geometry of the problem. (3.14) shows that the condition for ϵ to be small is equivalent to the condition that there should be a clear separation of scales between z_o and H. The surface roughness could also be modelled as a part of the distributed force. Therefore a clear separation of scales between z_o and H is required for the surface roughness to be treated consistently as a roughness length rather than as a force distribution.

Equation of (3.9) and (3.14) gives a relation between ϵ and kl:

$$\frac{kl}{\epsilon} = \frac{\ln(H/z_o)}{\ln(l/z_o)} = 1 + \frac{\ln(H/l)}{\ln(l/z_o)} = \frac{1}{1 - \epsilon \ln(H/l)}. \tag{3.15}$$

Hence $kl = O(\epsilon)$ as long as $1 - \epsilon \ln(H/l) = O(1)$, which is true unless l is as small as $O(z_o)$. Typically the smallest significant wavelengths of the force distribution are $O(H)$, and for such small scales $l \sim \lambda = O(H)$. Overall, therefore, it is safe to scale $kl = O(\epsilon)$, which shows that ϵ also characterises the ratio of vertical to horizontal length scales in the inner region.

3.3.4 Subdividing the inner region

A velocity scale for the inner region is defined by

$$U_l \equiv U(l) = \epsilon \ln \frac{l}{z_o} \tag{3.16}$$

and then the incident velocity in the inner region may be written

$$U(z) = U_l + \epsilon \ln \frac{z}{l}. \tag{3.17}$$

Hence $U(z) = U_l + O(\epsilon)$ throughout the inner region except very near the ground where $z \sim z_o$. Therefore the inner region is divided into two sub-layers. In the inner surface layer (ISL), $z \sim z_o$, the natural $O(1)$ vertical coordinate is $\zeta_i \equiv z/z_o$ and the incident velocity profile is $U(z) = \epsilon \ln \zeta_i = O(\epsilon)$. The shear stress layer (SSL) is defined as the rest of the inner region. Here the $O(1)$ vertical coordinate is $\zeta \equiv z/l$ and the incident velocity is $U(z) = U_l + O(\epsilon)$. The need to subdivide the inner region in this way was first recognised by Sykes (1980) and will be clarified in §§3.5.2–3.5.3.

3.4 Effects of strong force gradients

The remark made in §3.1, that rapidly varying force distributions can make turbulent stresses significant outside of the thin stress layer near the ground, is a manifestation of the fact that a *distributed* force can impose new vertical length scales upon the flow. Since the basic physics of distributed body forces is that force gradients create vorticity (§2.2), new length scales are most clearly defined by locations within the force distribution where the force gradient is strong.

When significant new vertical length scales exist, a mathematical problem for the SML analysis arises because the asymptotic flow structure of §3.3 implicitly ignore all vertical length scales except height above the ground. Although a general force distribution may have several places where the force gradient $\partial f/\partial z$ becomes large, the issues involved are demonstrated most clearly by consideration of a force distribution that is slowly varying up to a height h and zero above h, so that there is a single discontinuous change in distributed force at $z = h$.

3.4.1 Mathematical resolution of flow discontinuities in the outer region

The analysis of chapter 2 showed that in *inviscid* flow force discontinuities at height h lead to discontinuities in the streamwise velocity at height h. This result is equally valid for a force discontinuity in the outer region of the proposed turbulent flow structure. Therefore, given the dependence (3.9) of inner region height l on wavenumber k, for any height h there will be a range of wavenumbers such that the discontinuity lies in the outer region. Hence the Fourier components of perturbation velocity in this wavenumber range will be discontinuous at $z = h$.

Such unphysical flow discontinuities betray a limitation of the asymptotic flow structure as described in §3.3. What happens physically is that in any region of high flow gradients, turbulent stresses become large and dynamically important. Mathematically, therefore, turbulent stresses must be retained in the governing equations near any point of potential discontinuity. To reflect this, the asymptotic flow structure must be modified so as to include new turbulent stress layers around any height where strong force gradients occur outside the inner region.

Hence the analysis of the SML model is presented in two parts. The slowly varying analysis of §3.5 is valid at smaller wavenumbers for which any strong force gradients lie well within the inner region. The rapidly varying analysis of §3.6 considers the idealised case of a uniform force distribution which vanishes discontinously at a height within the outer region, for which a new shear stress layer is added to the flow structure around the discontinuity. By comparing the analyses of §3.5 and §3.6, it becomes clear how their results can be blended together to allow a practical treatment of any number of force discontinuities anywhere within the flow domain.

3.4.2 Effect of a strong elevated shear layer on turbulence

As well as the asymptotic flow structure, the SML turbulence model also ignores any vertical length scales other than height above the ground. This is a physical limitation of the SML model that is addressed by the more general DML turbulence model in

the analysis of §3.8.

3.5 Analysis of slowly varying force distributions

3.5.1 Governing equations

We begin with the steady, incompressible, Reynolds averaged Navier Stokes equations for total (*i.e.* undisturbed + perturbation) pressure, velocities and turbulent stresses, supplemented by a distributed force in the streamwise momentum equation:

$$\rho\hat{\mathbf{u}}^* \cdot \nabla^*\hat{\mathbf{u}}^* + \nabla^*\hat{p}^* = \nabla^* \cdot \hat{\boldsymbol{\tau}}^* - \mathbf{i}f^*, \tag{3.18}$$

$$\nabla^* \cdot \hat{\mathbf{u}}^* = 0. \tag{3.19}$$

The total velocity is the sum of the undisturbed streamwise flow $(U^*, 0)$ and the perturbation velocities (u^*, w^*) due to the force $\mathbf{i}f^*$. Similarly, $\hat{p}^* = P^* + p^*$ and $\hat{\boldsymbol{\tau}}^* = \boldsymbol{T}^* + \boldsymbol{\tau}^*$, but in the undisturbed boundary layer there are no gradients of pressure or turbulent stress, so the constant pressure P^* is dynamically irrelevant and the constant stress tensor $\boldsymbol{T}^*$ serves only to define the friction velocity u_*. Expanding flow quantities into their undisturbed and perturbation parts, neglecting the normal turbulent stress perturbations, and linearising the inertia terms by assuming that $|\mathbf{u}^*(z^*)| \ll U^*(z^*)$, we obtain in component form

$$\rho U^*\frac{\partial u^*}{\partial x^*} + \rho w^*\frac{\partial U^*}{\partial z^*} + \frac{\partial p^*}{\partial x^*} = \frac{\partial \tau^*}{\partial z^*} - f^*, \tag{3.20}$$

$$\rho U^*\frac{\partial w^*}{\partial x^*} + \frac{\partial p^*}{\partial z^*} = \frac{\partial \tau^*}{\partial x^*}, \tag{3.21}$$

$$\frac{\partial u^*}{\partial x^*} + \frac{\partial w^*}{\partial z^*} = 0. \tag{3.22}$$

The coordinates and physical quantities in these equations are non-dimensionalised using the characteristic length and velocity scales defined in §3.2:

$$k^* = k/L^*, \qquad \mathbf{x}^* = L^*\mathbf{x},$$

$$U^* = U_o^* U, \qquad f^* = \rho U_o^{*2} f/L^*, \tag{3.23}$$

$$\mathbf{u}^* = U_o^*\mathbf{u}, \qquad p^* = \rho U_o^{*2} p, \qquad \tau_{ij}^* = \rho u_*^2 \tau_{ij}.$$

The non-dimensionalised equations read

$$U\frac{\partial u}{\partial x} + w\frac{\partial U}{\partial z} + \frac{\partial p}{\partial x} = \epsilon^2\kappa^2\frac{\partial \tau}{\partial z} - f, \tag{3.24}$$

$$U\frac{\partial w}{\partial x} + \frac{\partial p}{\partial z} = \epsilon^2\kappa^2\frac{\partial \tau}{\partial x}, \tag{3.25}$$

$$\frac{\partial u}{\partial x} + \frac{\partial w}{\partial z} = 0. \tag{3.26}$$

The factor $\epsilon^2\kappa^2 = (u_*/U_o^*)^2$ appears here because the stress and inertia terms are non-dimensionalised using different velocity scales. Now the physical quantities in (3.24)–(3.26) are expressed in terms of their Fourier transforms, for example

$$u(x,z) = \int_{-\infty}^{\infty} u(k,z)e^{ikx}dk. \tag{3.27}$$

Note that a physical quantity is represented by the same symbol in both real and Fourier space; where there is any ambiguity as to whether the real space or Fourier space quantity is intended, the intention is clarified by writing the argument list explicitly as in (3.27). After a set of transformations like (3.27), (3.24)–(3.26) become

$$ikUu + wU' + ikp = \epsilon^2\kappa^2\tau' - f, \tag{3.28}$$

$$ikUw + p' = \epsilon^2\kappa^2 ik\tau, \tag{3.29}$$

$$iku + w' = 0. \tag{3.30}$$

Here the primes denote vertical differentiation $\partial/\partial z$.

Throughout the analysis that follows, it is convenient to assume that the wavenumber k is non-negative; this saves a lot of notational trouble involving $|k|$ and $\operatorname{sgn} k$. This assumption is not restrictive since $u(x,z)$, $p(x,z)$ etc. are real, and so their Fourier transforms for negative k may be obtained from those for non-negative k via the Hermitian relationship $u(-k) = [u(k)]^*$ (where the asterisk *here* denotes complex conjugation).

It is not possible to solve (3.28)–(3.30) exactly. Further progress must be made by considering the behaviour of (3.28)–(3.30) in each layer of the flow structure defined in §3.3 and applying the turbulence closure and approximations that are appropriate to each layer.

3.5.2 The shear stress layer

The natural vertical coordinate for the shear stress layer is $\zeta \equiv z/l$. Turbulent shear stresses are modelled by the eddy viscosity closure (3.3), which after non-dimensionalisation (3.23) takes the form

$$\tau = \frac{2z}{\epsilon}\frac{\partial u}{\partial z}. \tag{3.31}$$

Rewriting (3.28)–(3.30) in terms of ζ, making use of this turbulence closure, and writing the incident wind velocity as $U = U_l + \epsilon \ln \zeta$, we obtain

$$ikl(U_l + \epsilon \ln \zeta)u + \epsilon w/\zeta + iklp = 2\epsilon\kappa^2(\zeta u')' - lf, \tag{3.32}$$

$$ikl(U_l + \epsilon \ln \zeta)w + p' = 2ikl\epsilon\kappa^2\zeta u', \tag{3.33}$$

$$iklu + w' = 0. \tag{3.34}$$

Recall that kl, which multiplies many of the terms here, is $O(\epsilon)$. These equations are to be solved asymptotically in the limit $\epsilon \to 0$. The perturbation velocities and pressure are expanded as asymptotic series in ϵ:

$$u = u_o + \epsilon u_1 + \epsilon^2 u_2 + \cdots \tag{3.35}$$

$$w = \epsilon w_1 + \epsilon^2 w_2 + \cdots \tag{3.36}$$

$$p = p_o + \epsilon p_1 + \epsilon^2 p_2 + \cdots \tag{3.37}$$

The continuity equation (3.34) shows that there is no leading order vertical velocity perturbation, hence w_o has been omitted. The vertical momentum equation (3.33) shows that any pressure variation in the SSL must be $O(\epsilon^2)$; hence $p_o' = p_1' = 0$.

There are two mechanisms which give rise to a pressure perturbation in turbulent flow through a distributed force. The first is an inviscid mechanism. In the inviscid analysis, we found that the flow perturbations can be characterised as outflow from a source balanced by a constant velocity deficit in the wake of the force distribution. A pressure perturbation is associated with the source flow part of the inviscid solution. In the turbulent flow analysis, the outer region is quasi-inviscid and we shall see that a large part of the inner region also acts inviscidly, so this inviscid mechanism for

pressure perturbation is just as important for turbulent flow as it is for inviscid flow. A simple scaling analysis shows that this inviscid pressure perturbation is $O(fH/r)$, where r is the distance in real space from the measurement point to the centroid of the force distribution (the apparent origin of the source flow); this is formally $O(1)$ so far as our asymptotic expansion in ϵ is concerned.

The second mechanism is due to turbulent stress effects in the inner region, which give rise to an extra vertical velocity perturbation at $z \approx l$. This extra vertical velocity perturbation appears to the outer region like a wavy surface. An associated pressure perturbation is induced in the outer region, in the same way as in hill flow, and this pressure is transmitted back to the inner region. The extra vertical velocity at $z \approx l$ turns out, however, to be $O(\epsilon^2)$, so the corresponding pressure perturbation is much weaker then that produced by the inviscid mechanism.

Substituting (3.35)–(3.37) into (3.32)–(3.34) we can identify the following equations at $O(\epsilon)$ and $O(\epsilon^2)$:

$$iklU_l u_o - 2\epsilon\kappa^2(\zeta u_o')' = -lf - iklp_o, \tag{3.38}$$

$$iklU_l u_1 - 2\epsilon\kappa^2(\zeta u_1')' = -ikl u_o \ln\zeta - \epsilon w_1/\zeta - iklp_1, \tag{3.39}$$

$$p_o' + \epsilon p_1' = 0, \tag{3.40}$$

$$iklU_l w_1 + \epsilon p_2' = 2ikl\kappa^2\zeta u_o', \tag{3.41}$$

$$ikl u_o + \epsilon w_1' = 0, \tag{3.42}$$

$$ikl u_1 + \epsilon w_2' = 0. \tag{3.43}$$

The first of these equations governs the leading order streamwise perturbation velocity u_o. By means of a change of variables, defining the new Bessel function coordinate Z by

$$Z \equiv e^{3i\pi/4}\sqrt{\frac{2U_l kl\zeta}{\epsilon\kappa^2}}, \tag{3.44}$$

(3.38) is transformed into the Bessel equation

$$u_o'' + \frac{u_o'}{Z} + u_o = \frac{if}{kU_l} - \frac{p_o}{U_l}. \tag{3.45}$$

Solutions to (3.45) are expressed in terms of the Bessel functions $J_o(Z)$ and $K_o(-iZ)$ (Abramowitz & Stegun 1972, chapter 9). This somewhat unusual combination is advantageous for two reasons. Firstly, $J_o(Z)$ and $K_o(-iZ)$ are respectively exponentially large and exponentially small as $|Z| \to \infty$, which is useful when matching with the outer region. Secondly, $J_o(Z)$ and $K_o(-iZ)$ are related to the Kelvin functions: $J_o(Z) = \mathrm{ber}(\mathcal{Z}) + i\,\mathrm{bei}(\mathcal{Z})$ and $K_o(-iZ) = \mathrm{ker}(\mathcal{Z}) + i\,\mathrm{kei}(\mathcal{Z})$ where $\mathcal{Z} \equiv Z\exp(-3i\pi/4) = |Z|$, which is useful in practical implementations of the theory because $\mathrm{ber}(\mathcal{Z})$ etc. are real.

The general solution of (3.45) is

$$\begin{aligned} u_o &= A_o J_o(Z) + B_o K_o(-iZ) - \frac{p_o}{U_l} \\ &\quad + \frac{i}{kU_l}\int_{Z_o}^{Z} Z' f(z')\left\{J_o(Z)K_o(-iZ') - J_o(Z')K_o(-iZ)\right\} dZ', \end{aligned} \tag{3.46}$$

where A_o and B_o are to be determined by matching with the inner surface layer below and the outer region above. The SSL and outer region coordinates are related to each other by $\zeta = kz/(kl) = kz \times O(\epsilon^{-1})$, so an $O(1)$ coordinate for the matching region is given by

$$\chi = \epsilon^{-\alpha} kz \qquad \text{where} \qquad 0 < \alpha < 1. \tag{3.47}$$

In the matching region $|Z|$ therefore becomes large like $\epsilon^{\alpha-1}$, so the terms in (3.46) containing $J_o(Z)$ are exponentially large as $\epsilon \to 0$. Anticipating that there are no exponentially large terms in the outer region solution to match this behaviour, it follows that the coefficients in (3.46) of $J_o(Z)$ must cancel as $|Z| \to \infty$. This matching condition fixes A_o:

$$A_o + \frac{i}{kU_l}\int_{Z_o}^{\infty} Z' f(z') K_o(-iZ') dZ' = 0. \tag{3.48}$$

At $O(\epsilon)$ the governing equation for u_1 is (3.39). The general solution is

$$\begin{aligned} u_1 &= A_1 J_o(Z) + B_1 K_o(-iZ) - \frac{p_1}{U_l} \\ &\quad + \frac{i}{kU_l}\int_{Z_o}^{Z} Z' \left(f_1^{(\mathrm{U})} + f_1^{(\mathrm{w})}\right)\left\{J_o(Z)K_o(-iZ') - J_o(Z')K_o(-iZ)\right\} dZ', \end{aligned} \tag{3.49}$$

where $f_1^{(\mathrm{U})} \equiv iku_o \ln\zeta$ and $f_1^{(\mathrm{w})} \equiv \epsilon w_1/z$. The particular integrals in (3.49) are formally the same as additional force distributions, so we could think of the corrections as contributing to an effective total force distribution

$$f_{\mathrm{eff}} = f + \epsilon f_1^{(\mathrm{U})} + \epsilon f_1^{(\mathrm{w})} + \epsilon^2 f_2 + \cdots. \tag{3.50}$$

The leading order pressure p_o is determined by the original force distribution f, and in the same way the first order pressure perturbation may be split into two parts and ascribed to $f_1^{(\mathrm{U})}$ and $f_1^{(\mathrm{w})}$. Thus the first order streamwise velocity u_1 can be divided into three components:

$$u_1 \equiv u_1^{(\mathrm{cf})} + u_1^{(\mathrm{U})} + u_1^{(\mathrm{w})}, \tag{3.51}$$

where

$$u_1^{(\mathrm{cf})} = B_1 K_o(-iZ), \tag{3.52}$$

$$u_1^{(\mathrm{U})} = A_1^{(\mathrm{U})} J_o(Z) - \frac{p_1^{(\mathrm{U})}}{U_l} + \frac{i}{kU_l}\int_{Z_o}^{Z} Z' f_1^{(\mathrm{U})} \left\{J_o(Z)K_o(-iZ') - J_o(Z')K_o(-iZ)\right\} dZ', \tag{3.53}$$

$$u_1^{(\mathrm{w})} = A_1^{(\mathrm{w})} J_o(Z) - \frac{p_1^{(\mathrm{w})}}{U_l} + \frac{i}{kU_l}\int_{Z_o}^{Z} Z' f_1^{(\mathrm{w})} \left\{J_o(Z)K_o(-iZ') - J_o(Z')K_o(-iZ)\right\} dZ'. \tag{3.54}$$

Then $A_1^{(\mathrm{U})}$ and $A_1^{(\mathrm{w})}$ are determined by equations similar to (3.48), while B_1 is to be determined by matching with the ISL.

3.5.3 The inner surface layer

In the inner surface layer the natural vertical coordinate is $\zeta_i \equiv z/z_o$. Using the turbulence closure (3.31) and rewriting (3.28)–(3.30) in terms of the ISL coordinate ζ_i, we obtain

$$ikz_oUu + \epsilon w/\zeta_i + ikz_o p = 2\epsilon\kappa^2(\zeta_i u')' - z_o f, \tag{3.55}$$

$$ikz_oUw + p' = 2\epsilon\kappa^2 ikz_o\zeta_i u', \tag{3.56}$$

$$ikz_o u + w' = 0, \tag{3.57}$$

primes now indicate differentiation with respect to ζ_i. From (3.12) and (3.14) we can calculate the order of kz_o:

$$kz_o = \frac{kl}{l/z_o} \leq \epsilon e^{-U_l/\epsilon}, \tag{3.58}$$

i.e. kz_o is exponentially small as $\epsilon \to 0$. We could therefore solve (3.55)–(3.57) for the perturbation velocities and pressure expressed as asymptotic series in the small parameter kz_o. However, the SSL analysis contains only algebraically small corrections; hence there will be nothing small enough to match any $O(kz_o)$ corrections from the ISL. It is sufficient therefore to calculate only the leading order ISL solution, which should match the leading order solution in the SSL and all its algebraically small corrections (Belcher 1990).

To obtain the leading order solution (denoted by the subscript i) we neglect all terms that are $O(kz_o)$. The streamwise momentum equation reduces to

$$2\epsilon\kappa^2(\zeta_i u_i')' = z_o f. \tag{3.59}$$

When integrated once (3.59) gives the ISL shear stress:

$$\tau_i = \frac{2z}{\epsilon}\frac{\partial u_i}{\partial z} = \tau_w + \frac{1}{\epsilon^2\kappa^2}\int_{z_o}^{z} f(z')dz'. \tag{3.60}$$

The turbulent stress above a group of obstacles is transmitted to the ground partly through obstacle drag and partly through shear stresses at the ground. (3.60) describes the transfer of drag force between these two mechanisms in the absence of other dynamical contributions to the streamwise momentum balance. A second integration gives the leading order streamwise velocity:

$$u_i = \frac{\epsilon\tau_w}{2}\ln\frac{z}{z_o} + \frac{1}{2\epsilon\kappa^2}\int_{z_o}^{z} f(z')\ln\frac{z}{z'}dz'. \tag{3.61}$$

Reynolds stress gradients are of great practical importance in determining near-surface transport processes such as heat transfer and deposition of pollutants. In the absence of any force in the ISL, (3.60) shows that the turbulent shear stress is constant across the layer. But the ISL is a transcendentally thin layer, so the constancy of τ_i does not exclude the possibility of *algebraically large* stress gradients existing in the

ISL. The unscaled streamwise momentum equation (3.28) gives

$$\epsilon^2\kappa^2\tau_i' = f + iku_i\epsilon \ln\frac{z}{z_o} - \frac{ik\epsilon}{z}\int_{z_o}^{z} u_i(z')\,dz' + ikp_i. \tag{3.62}$$

Substituting for the ISL streamwise perturbation u_i (3.61) and ignoring terms involved the distributed force f (which in practical flows is small very near the ground), we find that

$$\epsilon^2\kappa^2\tau_i' = \frac{ik\epsilon^2\tau_w}{2}\left[\ln^2\frac{z}{z_o} - \ln\frac{z}{z_o} + 1 - \frac{z_o}{z}\right] + ikp_i. \tag{3.63}$$

Equation (3.63), which was also obtained by Hunt *et al.* (1988a) by a different method, shows that there is an $O(1)$ turbulent stress gradient at the ground that matches the streamwise pressure gradient. In the leading order SSL solution this pressure gradient is balanced by the force distribution and streamwise accelerations and the most significant turbulent stress gradient is $O(\epsilon)$. Thus, following Hunt *et al.* (1988a), the ISL may be characterised as a layer where the stress gradient increases dramatically from $O(\epsilon)$ to $O(1)$, as the balance of streamwise momentum changes to meet the surface boundary condition.

3.5.4 Matching the ISL and SSL

To match (3.46) and (3.52)–(3.54) with the ISL solution (3.61), it is convenient to separate out the terms of the SSL solution that are non-zero at $z = z_o$:

$$\begin{aligned} u_o \;=\; & A_oJ_o(Z_o) + B_oK_o(-iZ_o) - \frac{p_o}{U_l} \\ & + A_o\{J_o(Z) - J_o(Z_o)\} + B_o\{K_o(-iZ) - K_o(-iZ_o)\} \\ & + \frac{i}{kU_l}\int_{Z_o}^{Z} Z'f(z')\{J_o(Z)K_o(-iZ') - J_o(Z')K_o(-iZ)\}\,dZ'. \end{aligned} \tag{3.64}$$

The ISL coordinate ζ_i is related to the SSL coordinate ζ by

$$\zeta_i = \frac{z}{z_o} = \frac{z}{l} \div \frac{z_o}{l} = \zeta e^{U_l/\epsilon}; \tag{3.65}$$

this shows that in the SSL, where $\zeta = O(1)$, the ISL coordinate would be very large, $O(\exp(U_l/\epsilon))$. An $O(1)$ coordinate ϕ for the ISL/SSL matching region is defined by

$$\phi \equiv \zeta e^{\alpha U_l/\epsilon} \qquad \text{where} \qquad 0 \le \alpha \le 1. \tag{3.66}$$

($\alpha = 0$ gives $\phi = \zeta$, placing us in the SSL, while $\alpha = 1$ gives $\phi = \zeta_i$, placing us in the ISL, so an intermediate value of α corresponds to a matching region between these two layers.) In the matching region, $|Z| \sim \zeta^{\frac{1}{2}}$ is exponentially small like $\exp(-\alpha U_l/(2\epsilon))$, so it is appropriate to use small argument expansions (Abramowitz & Stegun 1972, §§9.6 and 9.1) for the Bessel functions in (3.64):

$$J_o(Z) = 1 - \frac{1}{4}Z^2 + O(Z^4), \tag{3.67}$$

$$K_o(-iZ) = -\left\{\gamma + \ln\frac{-iZ}{2}\right\}\left\{1 - \frac{Z^2}{4}\right\} - \frac{Z^2}{4} + O(Z^4, Z^4 \ln Z). \tag{3.68}$$

Using these small argument expansions for the non-constant terms in (3.64), we find that the leading order SSL solution in the matching region takes the form

$$u_o \approx A_o J_o(Z_o) + B_o K_o(-iZ_o) - \frac{p_o}{U_l} - \frac{B_o}{2}\ln\frac{z}{z_o} + \frac{1}{2\epsilon\kappa^2}\int_{z_o}^{z} f(z')\ln\frac{z}{z'}\,dz'. \tag{3.69}$$

Similarly, the first order corrections become

$$u_1^{(\mathrm{cf})} \approx B_1 K_o(-iZ_o) - \frac{B_1}{2}\ln\frac{z}{z_o}, \tag{3.70}$$

$$u_1^{(\mathrm{U})} \approx A_1^{(\mathrm{U})} J_o(Z_o) - \frac{p_1^{(\mathrm{U})}}{U_l} + \frac{1}{2\epsilon\kappa^2}\int_{z_o}^{z} f_1^{(\mathrm{U})}(z')\ln\frac{z}{z'}\,dz', \tag{3.71}$$

$$u_1^{(\mathrm{w})} \approx A_1^{(\mathrm{w})} J_o(Z_o) - \frac{p_1^{(\mathrm{w})}}{U_l} + \frac{1}{2\epsilon\kappa^2}\int_{z_o}^{z} f_1^{(\mathrm{w})}(z')\ln\frac{z}{z'}\,dz', \tag{3.72}$$

The highest order term of the ISL solution (3.61) is $O(\epsilon)$. Hence matching with the ISL means that all the $O(1)$ or higher terms of (3.69)–(3.72) must add to zero. Now $K_o(-iZ_o) \sim \ln(z_o/l) = O(\epsilon^{-1})$, so part of the $u_1^{(\mathrm{cf})}$ correction becomes $O(1)$ as $z/l \to 0$ and contributes to this leading order match:

$$A_o J_o(Z_o) + (B_o + \epsilon B_1) K_o(-iZ_o) - \frac{p_o}{U_l} = 0. \tag{3.73}$$

In (3.73), A_o, $J_o(Z_o)$, B_o, B_1, p_o and U_l are all $O(1)$, while $K_o(-iZ_o)$ is $O(\epsilon^{-1})$; at $O(\epsilon^{-1})$ it follows that $B_o = 0$ and hence that we must reject the term in $K_o(-iZ)$ as a part of the leading order solution. The remaining terms of (3.73), namely

$$A_o J_o(Z_o) + \epsilon B_1 K_o(-iZ_o) - \frac{p_o}{U_l} = 0, \tag{3.74}$$

determine the first order coefficient B_1 in terms of A_o and p_o.

Since all corrections in the ISL are exponentially small, it is necessary to show that the leading order solution in the ISL matches the leading order solution and all its algebraically small corrections in the SSL. For this purpose it is convenient to lump together all contributions to an additional distributed force for the first order correction—

$$f_1 = f_1^{(\mathrm{U})} + f_1^{(\mathrm{w})}, \quad p_1 = p_1^{(\mathrm{U})} + p_1^{(\mathrm{w})}, \quad A_1 = A_1^{(\mathrm{U})} + A_1^{(\mathrm{w})} \tag{3.75}$$

—and similarly for all higher order corrections. The nth order corrections are given by a set of equations like (3.70)–(3.72) and matching at $O(\epsilon^n)$ with the ISL and with the outer region gives

$$A_n J_o(Z_o) + \epsilon B_{n+1} K_o(-iZ_o) - \frac{p_n}{U_l} = 0, \tag{3.76}$$

$$A_n + \frac{i}{kU_l}\int_{Z_o}^{\infty} Z' f_n(z') K_o(-iZ')\, dZ' = 0. \tag{3.77}$$

There are algebraic contributions to the ground shear stress from all orders:

$$\tau_w = -B_1 - \epsilon B_2 - \epsilon^2 B_3 - \cdots \tag{3.78}$$

$$= -\frac{1}{\epsilon^2\kappa^2}\int_{z_o}^{\infty} f(z')\frac{K_o(-iZ')}{K_o(-iZ_o)}\, dz' - \frac{p_o}{\epsilon U_l K_o(-iZ_o)} + O(\epsilon). \tag{3.79}$$

Here we have used (3.48) and (3.74) to express the ground shear stress in terms of the distributed force and the inner region pressure p_o.

The shear stress gradient in the SSL is easily obtained by inspection of the streamwise momentum equations that u_o and u_1 satisfy; thus

$$\epsilon^2\kappa^2\frac{\partial \tau}{\partial z} = ikU(u_o + \epsilon u_1) + f + ik(p_o + \epsilon p_1) + \epsilon w_1 U' - \epsilon^2 ik \ln\zeta u_1 + O(\epsilon^2)$$

$$= ikUu + f + ikp + wU' + O(\epsilon^2). \tag{3.80}$$

It follows that u_o and u_1 have associated stress gradients which match the ISL stress gradient to $O(\epsilon^2)$; clearly the stress gradient of the next order velocity perturbation u_2 will improve the match to $O(\epsilon^3)$, and so on.

Finally we consider the particular integrals over distributed force f that appear in (3.61) and (3.69), and the additional force integrals that contribute to higher order corrections like (3.71). The former integrals match exactly. Corrections arising from the latter integrals are algebraically small within the SSL, but become exponentially small in the ISL/SSL matching region. Note that all contributions to additional distributed forces contain the factor k. Then in the matching region defined by (3.66) the typical force integral becomes

$$\int_{z_o}^{z} f_n(z') \ln \frac{z}{z'}\, dz' = kle^{-\alpha U_l/\epsilon} \int_{\phi_o}^{\phi} k^{-1} f_n(\phi') \ln \frac{\phi}{\phi'}\, d\phi' = O(\epsilon e^{-\alpha U_l/\epsilon}), \qquad (3.81)$$

which is exponentially small. Hence the only $O(\epsilon^n)$ SSL corrections that remain $O(\epsilon^n)$ in the matching region are contributions to the constant turbulent stress and are matched by the ISL's τ_w as given by (3.78).

Jackson & Hunt (1975), in their analysis of flow over a low hill, did not subdivide their inner region, but instead used solutions like those of the SSL here all the way down to the ground. Consider applying the ground boundary condition $u(z_o) = 0$ to the SSL solution. At $O(1)$, (3.46) gives

$$A_o + B_o K_o(-iZ_o) - p_o/U_l = 0. \qquad (3.82)$$

A_o, B_o, p_o and U_l are by definition $O(1)$, but $K_o(-iZ_o) \sim \ln l/z_o = O(\epsilon^{-1})$. Hence B_o must be zero. Since A_o and p_o are not free to be determined by (3.82) with $B_o = 0$, it follows that the leading order SSL solution cannot satisfy $u_o(z_o) = 0$. Hence the need for an inner surface layer very close to the ground.

Put more formally, the SSL solution cannot satisfy the ground boundary condition because the ground at $z = z_o$ lies far below the region where the definition of the SSL, $z/l = O(1)$, is reasonable. In the SSL, functions of the $O(1)$ layer coordinates ζ and Z ought themselves to be $O(1)$; but as $z \to z_o$ we have $\zeta = z/l = O(\exp(-U_l/\epsilon)) \ll O(1)$ and consequently $K_o(-iZ) = O(\epsilon^{-1}) \gg O(1)$.

Therefore, as first recognised by Sykes (1980) and later developed by Hunt *et al.* (1988a), correct treatment of the ground boundary condition is impossible without an ISL analysis.

3.5.5 SSL shear stress and vertical velocity perturbations

The scaling of shear stress means that nth order streamwise velocity perturbations are associated via the turbulence closure model (3.31) with $(n-1)$th order shear stress perturbations. Thus the shear stress perturbation τ is expanded as

$$\tau = \epsilon^{-1}\tau_{-1} + \tau_o + \epsilon\tau_1 + \cdots. \tag{3.83}$$

By differentiation of (3.45) (with $B_o = 0$) and (3.70), the shear stress profiles associated with u_o and $u_1^{(\mathrm{cf})}$ are

$$\tau_{-1} = -A_o Z J_1(Z) - \frac{iZ}{kU_l}\int_{Z_o}^{Z} Z' f(z')\left\{J_1(Z)K_o(-iZ') + iJ_o(Z')K_1(-iZ)\right\} dZ', \tag{3.84}$$

$$\tau_o^{(\mathrm{cf})} = iB_1 Z K_1(-iZ). \tag{3.85}$$

The corresponding vertical velocity perturbations are conveniently calculated by using continuity to rewrite the streamwise momentum equations as

$$-\epsilon U_l w_1' - \epsilon\kappa^2\tau_{-1}' = -ikl p_o - lf, \tag{3.86}$$

$$-\epsilon U_l w_2'^{(\mathrm{cf})} - \epsilon\kappa^2\tau_o'^{(\mathrm{cf})} = 0. \tag{3.87}$$

Hence by integration,

$$\epsilon U_l w_1 = ikp_o(z - z_o) + \int_{z_o}^{z} f(z')\,dz' - \epsilon\kappa^2\{\tau_{-1} + A_o Z_o J_1(Z_o)\}, \tag{3.88}$$

$$\epsilon U_l w_2^{(\mathrm{cf})} = -\epsilon\kappa^2\{\tau_o^{(\mathrm{cf})} - iB_1 Z_o K_1(-iZ_o)\}. \tag{3.89}$$

At the top of the inner region, where the shear stresses τ_{-1} and $\tau_o^{(\mathrm{cf})}$ decay exponentially, equation (3.88) shows that there is no first order contribution to the vertical velocity from Reynolds stress effects. This means that although turbulent stress effects are important at leading order *within* the SSL, they make no contribution to the leading order match with the outer region. The terms in (3.88) which do contribute to a vertical velocity at the top of the inner region represent purely inviscid behaviour. At second order Reynolds stress effects produce a perturbation vertical velocity whose limiting value is

$$\epsilon^2 w_2^{(\mathrm{cf})} \to i\epsilon^2\kappa^2 B_1 Z_o K_1(-iZ_o)/U_l \approx -\epsilon^2\kappa^2 B_1/U_l \approx \epsilon^2\kappa^2\tau_w/U_l. \tag{3.90}$$

3.5.6 Discussion of the inner region solutions

The leading order solutions $\{u_o, \tau_{-1}, w_1\}$ represent a largely inviscid response to the applied distributed force. Leading order Reynolds stresses are significant within the SSL but not at its lower or upper boundaries. The streamwise perturbation velocity u_o tends to a constant non-zero value as $z/l \to 0$, hence the leading order solution alone does not match with the ISL.

At $O(\epsilon)$ there are three first order corrections, labelled (cf), (U) and (w). The (cf) correction behaves logarithmically as $z/l \to 0$, giving a ground shear stress and combining with the leading order solution to match with the ISL. At leading order, therefore, the sum $u_o + \epsilon u_1^{(\mathrm{cf})}$ is a uniformly valid approximation for the complete inner region.

The (U) and (w) corrections are conveniently represented as perturbations resulting from additional distributed forces. They arise respectively from approximating the incident velocity $U(z)$ as a constant, $U(z) \approx U_l$, and from neglect of the $O(\epsilon)$ incident velocity shear dU/dz, and are calculated as the results of additional force distributions $\epsilon f_1^{(\mathrm{U})} \equiv \epsilon i k u_o \ln \zeta$ and $\epsilon f_1^{(\mathrm{w})} \equiv \epsilon^2 w_1 / z$.

Further evaluation of the general expressions (3.71) and (3.72), for the flow perturbations due to $f_1^{(\mathrm{U})}$ and $f_1^{(\mathrm{w})}$, is not attempted here since (i) the results would not be very illuminating and (ii) a practical implementation of this analysis can compute these expressions using the leading order results already presented (but for additional $O(\epsilon)$ force distributions). It will be necessary, however, to consider all the $O(\epsilon)$ corrections at the top of the inner region when matching with the outer region.

3.5.7 Analysis of the outer region

Take the curl of (3.28)–(3.30) and neglect the turbulent stress gradients, to obtain the governing equations for the outer region,

$$w'' - \left(k^2 + \frac{U''}{U}\right) w = \frac{f'}{U}, \tag{3.91}$$

$$ikU u + wU' + ikp = -f, \tag{3.92}$$

$$ikUw + p' = 0, \tag{3.93}$$

$$iku + w' = 0. \tag{3.94}$$

Equations (3.92)–(3.94) may be used to calculate the perturbation pressure and streamwise velocity once (3.91) has been solved for the vertical velocity w. For a logarithmic boundary layer, the incident shear term in (3.91) may be written

$$\frac{U''w}{U} = \frac{-\epsilon w}{z^2 U}, \tag{3.95}$$

so it is appropriate to solve (3.91) by writing w as an asymptotic series in ϵ:

$$w = w_o + \epsilon w_1 + \epsilon^2 w_2 + \cdots \tag{3.96}$$

Substitute (3.96) into (3.91) and group terms of similar order, then

$$w_o'' - k^2 w_o = \frac{f'}{U}, \tag{3.97}$$

$$w_1'' - k^2 w_1 = \frac{-w_o}{z^2 U}, \tag{3.98}$$

and so on. The general solution to (3.97) is

$$w_o = C_o e^{-kz} + D_o e^{kz} + \int_{z_o}^{z} \frac{f(z')\cosh k(z-z')}{U(z')}\,dz', \tag{3.99}$$

where the lower limit of the integral has been chosen for later convenience. Then by continuity the leading order streamwise velocity is

$$u_o = -iC_o e^{-kz} + iD_o e^{kz} + \frac{if}{kU} + i\int_{z_o}^{z} \frac{f(z')\sinh k(z-z')}{U(z')}\,dz', \tag{3.100}$$

and the leading order pressure is

$$p_o = \frac{if}{k} - Uu_o = iUC_o e^{-kz} - iUD_o e^{kz} - iU\int_{z_o}^{z} \frac{f(z')\sinh k(z-z')}{U(z')}\,dz'. \tag{3.101}$$

The constant D_o is determined by applying the upper boundary condition that w_o must be bounded as $kz \to \infty$. This means that the terms in $\exp(kz)$ must cancel each other above the force distribution, hence

$$D_o + \frac{1}{2}\int_{z_o}^{\infty} \frac{f(z')\exp(-kz')}{U(z')}\,dz' = 0. \tag{3.102}$$

It remains to determine the other constant C_o and the inner region pressure p_o by matching (3.99)–(3.101) with the corresponding SSL solutions.

At first order, (3.98) shows that the $O(\epsilon)$ vertical velocity correction can be represented as the result of a secondary force distribution ϵf_1 defined by

$$f_1' = -w_o/z^2. \tag{3.103}$$

This correction is similar to the (w) correction in the inner region.

3.5.8 Matching the inner and outer regions

The detailed matching of the inner and outer regions is analysed by focusing on the vertical velocity perturbation w. Matching is a two-part process. The complementary functions of the inner and outer solutions contain constants of integration that remain to be determined by matching and by applying boundary conditions. The particular integrals, on the other hand, are already fully specified. The matching process includes checking that the particular integrals are mutually consistent, which provides a useful check on the individual layer analyses.

The shear stress layer is defined by $z/l = O(1)$, so $kz = O(\epsilon)$ in the SSL, while in the outer region $kz = O(1)$. Therefore an $O(1)$ matching coordinate, χ, for the overlap region between the SSL and the outer region is defined by

$$kz = \epsilon^{\alpha}\chi, \qquad \text{where} \quad 0 \leq \alpha \leq 1. \tag{3.104}$$

Hence the outer region coordinate kz is small in the overlap region where $\chi = O(1)$. The SSL Bessel function coordinate Z in the overlap region is

$$Z = \frac{\exp(3i\pi/4)}{\kappa}\sqrt{\frac{2U_l kz}{\epsilon}} = \frac{\exp(3i\pi/4)}{\kappa}\sqrt{2U_l\chi}\,\epsilon^{\alpha/2-1}, \tag{3.105}$$

which is large.

Consider the behaviour of the SSL vertical velocities (3.88) and (3.89) in the overlap region. For large $|Z|$, $K_o(-iZ)$ and $K_1(-iZ)$ tend exponentially to zero while $J_o(Z)$ and $J_1(Z)$ become exponentially large. Thus $\tau_o^{(\mathrm{cf})}$ is negligible. τ_{-1} is also

negligible if the matching region lies above the top of the force distribution, since the $J_1(Z)$ terms in (3.84) cancel each other (this condition determines A_o).

If the matching region does contain any distributed force, τ_{-1} can be rewritten:

$$\tau_{-1} = \frac{iZJ_1(Z)}{kU_l}\int_Z^\infty Z' f(z') K_o(-iZ')\,dZ' + \frac{ZK_1(-iZ)}{kU_l}\int_{Z_o}^Z Z' f(z') J_o(Z')\,dZ'. \quad (3.106)$$

As discussed in §3.4, the present analysis applies to slowly varying force distributions for which any strong force gradients $\partial f/\partial z$ lie well within the inner region. Hence $f(z)$ does not vary rapidly in the matching region. Then the exponential behaviour of the Bessel functions in (3.106) means that the two integrals derive mainly from contributions very close to $Z' = Z$, and τ_{-1} can be evaluated approximately in the matching region by moving $f(z)$ outside the integrals. Hence (3.106) becomes

$$\tau_{-1} \approx \frac{Z_o J_1(Z_o) Z K_1(-iZ) f(z)}{kU_l}, \quad (3.107)$$

which is exponentially small. Hence τ_{-1} is also negligible in the matching region even if the force distribution extends above the inner region.

Thus the vertical velocity that matches at $O(\epsilon)$ and $O(\epsilon^2)$ with the outer region is

$$\epsilon w_1 + \epsilon^2 w_2^{(\mathrm{cf})} \approx \frac{ikp_o(z-z_o)}{U_l} + \int_{z_o}^z \frac{f(z')}{U_l}\,dz' + \frac{i\epsilon^2\kappa^2 B_1 Z_o K_1(-iZ_o)}{U_l}. \quad (3.108)$$

Similar arguments applied to u_o and $u_1^{(\mathrm{cf})}$ show that the SSL streamwise perturbation velocity for matching with the outer region is

$$u_o \approx \frac{if}{kU_l} - \frac{p_o}{U_l}, \quad (3.109)$$

which could equally have been obtained from (3.108) by continuity.

The inner/outer region matching is enhanced by consideration of the various $O(\epsilon)$ corrections to the inner and outer region solutions. In the outer region, the $O(\epsilon)$ correction due to neglect of incident velocity shear is represented as the result of an secondary force distribution given by (3.103). Noting the exponential behaviour of w_o, partial integration of (3.103) gives

$$f_1 = \frac{w_o}{z}\{1 + O(kz)\}; \quad (3.110)$$

hence as $kz \to 0$ the first order correction in the outer region matches with the (w) correction in the inner region. Therefore it is convenient to leave (3.110) and the inner region (w) correction to one side. Practical implementations of this analysis can calculate these corrections for the whole flow domain as the result of a uniformly valid additional force distribution defined by (3.103).

The inner region (cf) correction has already been shown to be negligible in the matching region. The inner region (U) correction is not negligible and has no counterpart in the outer region because it is not necessary to approximate $U(z)$ to obtain the outer region solutions. Therefore we calculate the effect of the (U) correction on the inner region solutions within the matching region. It is easiest to consider the streamwise velocity perturbation. Equation (3.109) shows that in the matching region,

$$u_1^{(\mathrm{U})} = \frac{if_1^{(\mathrm{U})}}{kU_l} - \frac{p_1^{(\mathrm{U})}}{U_l} = \frac{-u_o \ln(z/l)}{U_l} - \frac{p_1^{(\mathrm{U})}}{U_l}, \tag{3.111}$$

where the pressure perturbation $p_1^{(\mathrm{U})}$ is associated with the additional force $f_1^{(\mathrm{U})}$ in the same way as p_o arises from the imposed force distribution f. Therefore the corrected SSL solution in the matching region is

$$\begin{aligned} u_o + \epsilon u_1^{(\mathrm{U})} &= u_o\left(1 - \frac{\epsilon \ln(z/l)}{U_l}\right) - \frac{\epsilon p_1^{(\mathrm{U})}}{U_l} = \frac{u_o U_l}{U(z)} - \frac{\epsilon p_1^{(\mathrm{U})}}{U_l} + O(\epsilon^2) \\ &= \frac{if}{kU} - \frac{p_o}{U} + O(\epsilon), \end{aligned} \tag{3.112}$$

i.e. the effect of incorporating the (U) correction is to replace occurences of U_l by $U(z)$. This might have been anticipated simply because $U(z)$ varies much more slowly than the perturbation velocities u and w. Correcting the vertical velocity perturbations in a similar way (noting that $dU/dz = O(\epsilon)$), we obtain

$$\epsilon w_1 + \epsilon^2 w_2^{(\mathrm{cf})} + \epsilon^2 w_2^{(\mathrm{U})} \approx \frac{ikp_o(z - z_o)}{U} + \int_{z_o}^{z} \frac{f(z')}{U(z')}\, dz' + \frac{i\epsilon^2\kappa^2 B_1 Z_o K_1(-iZ_o)}{U}. \tag{3.113}$$

These solutions can now be matched with those in the outer region, each incorporating the same approximations and corrections.

The form of the outer region solutions in the matching region is obtained by

substituting the $O(1)$ coordinate χ into (3.99)–(3.101):

$$u_o^{(\mathrm{OR})} = i(D_o - C_o) + i\epsilon^\alpha (C_o + D_o)\chi + \frac{if}{kU} + O(\epsilon^{2\alpha}), \tag{3.114}$$

$$w_o^{(\mathrm{OR})} = C_o + D_o + \epsilon^\alpha (D_o - C_o)\chi + \int_{z_o}^{z} \frac{f(z')}{U(z')}\, dz' + O(\epsilon^{2\alpha}), \tag{3.115}$$

$$p_o^{(\mathrm{OR})} = iU(C_o - D_o) - i\epsilon^\alpha (C_o + D_o)\chi + O(\epsilon^{2\alpha}). \tag{3.116}$$

Comparison of (3.112) and (3.114), or of (3.113) and (3.115), shows that the particular force integrals already match at leading order. Then matching complementary functions in the inner and outer region solutions for perturbation velocities gives the following relations between C_o, D_o and the inner region pressure p_o:

$$C_o + D_o = \frac{i\epsilon^2 \kappa^2 B_1 Z_o K_1(-iZ_o)}{U_\alpha}, \tag{3.117}$$

$$i(C_o - D_o) = \frac{p_o}{U_\alpha}. \tag{3.118}$$

Here U_α is the characteristic velocity of the matching region. Together with the upper boundary condition (3.102), these relations determine all the remaining unknowns. We note that the $O(\epsilon^\alpha)$ linear term in (3.115) matches exactly the linear pressure term of the SSL solution (3.113), which in practice considerably improves the inner/outer region matching.

3.5.9 A uniformly valid approximation

The matching process shows that the constant and linear terms of the SSL vertical velocity match the first two terms of the Maclaurin expansion of the outer region's $C_o \exp(-kz) + D_o \exp(kz)$ for small kz. This suggests that a uniformly valid approximation may be formed by replacing the constant and linear terms of the SSL solution by $C_o \exp(-kz) + D_o \exp(kz)$ while retaining the other SSL terms that are important in the inner region but decay exponentially in the outer region:

$$w^{(\mathrm{UVA})} = C_o e^{-kz} + D_o e^{kz} + \int_{z_o}^{z} \frac{f(z') \cosh k(z - z')}{U_g(z')}\, dz' - \frac{\epsilon^2 \kappa^2 \tau^{(\mathrm{UVA})}}{U_l}, \tag{3.119}$$

where $\tau^{(\mathrm{UVA})} = \epsilon^{-1}\tau_{-1} + \tau_o^{(\mathrm{cf})}$. The "blend velocity" $U_g(z)$ is defined such that $U_g(z) \to U_l$ for $z \ll l$ and $U_g(z) \to U(z)$ for $z \gg l$; then the force integral in

(3.119) is a uniformly valid approximation to both inner and outer region particular integrals. A uniformly valid streamwise velocity perturbation may be obtained from (3.119) by continuity.

This approximation includes the leading order solution and all $O(\epsilon)$ corrections except that due to effects of incident velocity shear. Physically this correction accounts for the vertical displacement of upstream vorticity by $w^{(\mathrm{UVA})}$. It may be calculated as the leading order response to an extra distributed force $\epsilon f_1^{(\mathrm{w})} \equiv \epsilon w^{(\mathrm{UVA})}/z$.

3.6 Analysis of rapidly varying force distributions

In this second part of the SML analysis there is a strong force gradient outside the inner region, which was excluded from the analysis of §3.5 for the reasons discussed in §3.4.

3.6.1 A modified flow structure

If used incorrectly for a force distribution that is discontinuous in the outer region, the analysis of §3.5 gives a corresponding discontinuity in the streamwise perturbation velocity. In a real flow this is not permissible. What happens in practice is that regions of rapid variation locally create turbulent stresses that are dynamically important and must be included in the calculation, even though the flow outside these regions of rapid variation may behave inviscidly. Consequently the flow structure described in §3.3 must be modified to include new turbulent stress layers around any height where strong force gradients occur outside the inner region. Such a modified flow structure is illustrated in figure 3.2 for the case where just one new layer is required around the height h. In order to establish the precise effects of this new flow structure, it suffices to consider the canonical force distribution

$$\begin{aligned} f &= 1, \qquad z_o \le z \le h, \\ f &= 0, \qquad z > h. \end{aligned} \tag{3.120}$$

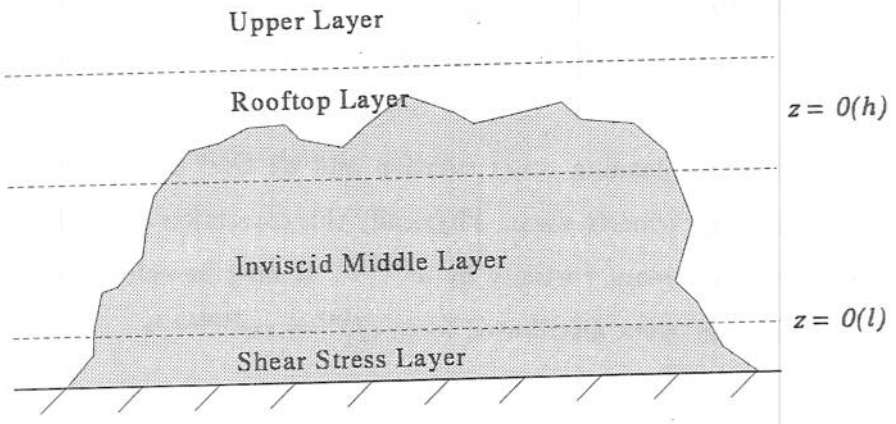

Figure 3.2: Modified flow structure for large wavenumbers such that $l \ll h$.

Much of the detailed analysis of the perturbations induced by this force distribution is similar to that of §3.5 and so will not be repeated unnecessarily. In the following subsections we concentrate on the differences from the analysis for slowly varying force distributions.

3.6.2 The inner surface and shear stress layers

The ISL and SSL analyses proceed as in §§3.5.3–3.5.6, but now the force is constant throughout these layers; hence uniformly valid solutions for the inner region are

$$\begin{aligned} u_o + \epsilon u_1^{(\mathrm{cf})} &= \epsilon B_1 K_o(-iZ) - \frac{p_o}{U_l} + \frac{i}{kU_l}\{1 + Z_o J_1(Z_o) K_o(-iZ)\}, \\ \epsilon w_1 + \epsilon^2 w_2^{(\mathrm{cf})} &= \frac{(ikp_o + 1)(z - z_o)}{U_l} - \frac{\epsilon^2\kappa^2(\tau_o^{(\mathrm{cf})} - iB_1 Z_o K_1(-iZ_o))}{U_l}, \end{aligned} \tag{3.121}$$

where

$$\tau_o^{(\mathrm{cf})} = iB_1 Z K_1(-iZ).$$

B_1 and p_o are related by the ISL/SSL matching condition (3.74) with

$$A_o = \frac{Z_o K_1(-iZ_o)}{kU_l}. \tag{3.122}$$

Thus as $z/l \to \infty$, the velocity perturbations that must match with the layer above, including the $\epsilon f_1^{(\mathrm{U})}$ corrections as in §3.5.8, are

$$u_o + \epsilon u_1^{(\mathrm{U})} \approx \frac{i}{kU} - \frac{p_o}{U} + O(\epsilon). \tag{3.123}$$

$$\epsilon w_1 + \epsilon^2 w_2^{(\mathrm{cf})} + \epsilon^2 w_2^{(\mathrm{U})} \approx \frac{(ikp_o + 1)(z - z_o)}{U} + \frac{i\epsilon^2\kappa^2 B_1 Z_o K_1(-iZ_o)}{U}. \tag{3.124}$$

3.6.3 The inviscid middle layer

Governing equations for the inviscid middle layer (IML) are the same as those used for the outer region analysis of §3.5.7. For a constant force, the general solutions are

$$w_o = C_o e^{-kz} + D_o e^{kz} + \int_{z_o}^{z} \frac{\cosh k(z - z')}{U(z')}\, dz', \tag{3.125}$$

$$u_o = -iC_o e^{-kz} + iD_o e^{kz} + \frac{i}{kU} + i\int_{z_o}^{z} \frac{\sinh k(z - z')}{U(z')}\, dz', \tag{3.126}$$

$$p_o = \frac{i}{k} - Uu_o = iUC_o e^{-kz} - iUD_o e^{kz} - iU\int_{z_o}^{z} \frac{\sinh k(z - z')}{U(z')}\, dz'. \tag{3.127}$$

Matching between the SSL and the IML proceeds exactly as between the inner and outer regions in §3.5.8, the only difference being that D_o is not yet determined. Hence the two matching conditions (3.117) and (3.118) link p_o, C_o and D_o as in §3.5. A third relation will follow from matching with the rooftop layer around $z \approx h$. To find the IML perturbations that match with the rooftop layer, the appropriate limiting process is $k(h - z) \to 0$. Therefore we substitute $kz = kh - \epsilon^\alpha \psi$, where $0 \le \alpha \le 1$ and $\psi = O(1)$, into (3.125)–(3.127) and obtain

$$w_o = C_o e^{-kh} + D_o e^{kh} + \epsilon^\alpha \psi (C_o e^{-kh} - D_o e^{kh}) - \frac{\epsilon^\alpha(\psi - \psi_o)}{kU_h} + O(\epsilon^{2\alpha}), \tag{3.128}$$

$$u_o = \frac{i}{kU_h} - iC_o e^{-kh} + iD_o e^{kh} + O(\epsilon^\alpha), \tag{3.129}$$

$$p_o = \frac{i}{k} - U_h u_o = iU_h C_o e^{-kh} - iU_h D_o e^{kh} + O(\epsilon^\alpha). \tag{3.130}$$

3.6.4 The rooftop layer

The rooftop layer (RL) requires new consideration. The effect of a discontinuity in f at $z = h$ is that the mean flow changes rapidly near $z = h$ and so turbulent stresses

become important in a region of the flow where they would otherwise be negligible. Mathematically, the shear stress gradient $\partial\tau/\partial z \approx \Delta\tau/\Delta z$ is large because the vertical length scale Δz over which the shear stress changes is smaller than it would otherwise be at a height h above the ground. Thus the rooftop layer is constructed by defining a new vertical coordinate relative to h and acknowledging that strong perturbation stress and velocity gradients may exist over distances that are $O(1)$ in the new coordinate.

To deduce the scaling of the new vertical coordinate ζ_h and the thickness of the rooftop layer, write

$$z = h + \epsilon^{\beta}\zeta_h/k, \tag{3.131}$$

$$U(z) \approx U_h + \epsilon^{\beta+1}\zeta_h/(kh). \tag{3.132}$$

These definitions are substituted into the streamwise momentum equation (3.32), which then becomes

$$ik\left(U_h + \frac{\epsilon^{\beta+1}\zeta_h}{kh}\right)u + \frac{\epsilon w}{h} + ikp = 2\epsilon^{1-2\beta}\kappa^2k^2hu'' + 2\epsilon^{1-\beta}\kappa^2k^2(\zeta_h u')' - f, \tag{3.133}$$

where the prime indicates differentiation with respect to ζ_h. Of the two stress terms on the right hand side of (3.133), the first is larger and is of similar order to the advection term when $kh\epsilon^{1-2\beta} = O(1)$. Hence the vertical thickness l_r of the rooftop layer is

$$l_r = \epsilon^{\beta}/k = O(\sqrt{\epsilon h/k}) \approx O(\sqrt{hl}). \tag{3.134}$$

At leading order the pressure across the RL is a constant, p_h, since $kl_r = O(\epsilon^{\beta})$. (Although it is not necessarily the same as the constant leading order pressure in the SSL, because pressure may vary dramatically across the inviscid middle layer.) Equation (3.133) shows that the vertical velocity term $\epsilon w/h$ is negligible as in the SSL but for a different reason. In the SSL the incident velocity shear ϵ/z may be large, but proximity to the ground means that w itself is small. In the RL w may be significant, in fact we know that u and w are of similar order in the inviscid layer below, but the incident velocity shear ϵ/h is very small. Thus the leading order form of (3.133) is identical to that of the SSL governing equation, except that the reference

velocity and pressure are different. At leading order the general solution is

$$u_o = h_2 K_o(-iY) - \frac{p_h}{U_h} + \frac{i}{kU_h}\int_{Y_h}^{Y} Y' f(z')\left\{J_o(Y)K_o(-iY') - J_o(Y')K_o(-iY)\right\} dY'. \tag{3.135}$$

The new coordinate Y is defined by

$$Y \equiv e^{3i\pi/4}\sqrt{\frac{2U_h kl\zeta}{\epsilon\kappa^2}}; \tag{3.136}$$

here Y is used rather than Z to emphasise that the velocity scale in the definition is U_h rather than U_l. A possible term in $J_o(Y)$ has been omitted from (3.135) because the particular integral has been written so as to vanish for $z > h$. Below $z = h$ (3.135) becomes

$$u_o = h_2 K_o(-iY) - \frac{p_h}{U_h} + \frac{i}{kU_h}\left\{i - Y_h K_1(-iY_h)J_o(Y) + iY_h J_1(Y_h)K_o(-iY)\right\}, \quad z < h. \tag{3.137}$$

The Bessel function coordinate Y is very large in the RL, since $h/l \gg 1$. It follows that the Bessel functions around $z \approx h$ are either growing or decaying exponentially. Moving downwards from $z = h$, the terms in $K_o(-iY)$ grow exponentially. Since there is no similar exponential behaviour for these terms to match in the IML, their coefficients must cancel each other:

$$h_2 + \frac{iY_h J_1(Y_h)}{kU_h} = 0. \tag{3.138}$$

Thus the RL solution for $z < h$ reduces to

$$u_o = \frac{1}{kU_h}\left\{i - Y_h K_1(-iY_h)J_o(Y)\right\} - \frac{p_h}{U_h}, \quad z < h, \tag{3.139}$$

while that for $z > h$ is

$$u_o = -\frac{iY_h J_1(Y_h)}{kU_h}K_o(-iY) - \frac{p_h}{U_h}, \quad z > h. \tag{3.140}$$

In (3.139), the Bessel function term decays exponentially like $\exp(\sqrt{z} - \sqrt{h})$ as the RL coordinate $\zeta_h \to -\infty$ for matching with the IML. Then matching the IML and

RL streamwise velocities proceeds as in earlier examples, to give the rooftop pressure p_h as

$$p_h = iU_h(C_o e^{-kh} - D_o e^{kh}). \tag{3.141}$$

The change in vertical velocity w across the RL due to the shear stress correction terms is

$$\begin{aligned}\Delta w^{(\mathrm{RL})} &= \frac{\epsilon\kappa^2 Y_h}{kU_h^2}\left\{-K_1(-iY_h)\left[Y'J_1(Y')\right]_{Y_o}^{Y_h} - iJ_1(Y_h)\left[-iY'K_1(-iY')\right]_{Y_h}^{\infty}\right\} \\ &= \frac{\epsilon\kappa^2 Y_h K_1(-iY_h)Y_o J_1(Y_o)}{kU_h^2},\end{aligned} \tag{3.142}$$

which is exponentially small on several counts. Therefore the limiting values of vertical perturbation velocity above and below the RL are equal. Hence the streamwise and vertical velocities above the RL are

$$u_o^{(\mathrm{RL})} = -p_h/U_h, \tag{3.143}$$

$$w_o^{(\mathrm{RL})} = C_o e^{-kh} + D_o e^{kh}. \tag{3.144}$$

These must match the upper layer solution given by

$$w_o^{(\mathrm{UL})} = g_1 e^{-kz}, \tag{3.145}$$

$$u_o^{(\mathrm{UL})} = -ig_1 e^{-kz}. \tag{3.146}$$

Hence the final matching conditions are

$$g_1 e^{-kh} = C_o e^{-kh} + D_o e^{kh}, \tag{3.147}$$

$$-ig_1 e^{-kh} = -p_h/U_h, \tag{3.148}$$

$$\Rightarrow\ i(C_o e^{-kh} + D_o e^{kh}) = p_h/U_h. \tag{3.149}$$

(3.141) and (3.149) together imply that $D_o = 0$ and that

$$p_h/U_h = iC_o e^{-kh} = e^{-kh} p_o/U_\alpha. \tag{3.150}$$

3.6.5 Comparison with a naive small k solution

By a "naive" solution we mean one which is obtained if we ignore the difficulties that motivated this large wavenumber analysis and blindly apply the small wavenumber solution of §3.5 to the current canonical force distribution. Substituting the canonical force distribution (3.120) into the uniformly valid small wavenumber solution (3.119), we obtain for $z < h$

$$\begin{aligned} w^{(\mathrm{UVA})} &= C_o e^{-kz} + D_o e^{kz} + \int_{z_o}^{z} \frac{\cosh k(z-z')}{U_g(z')}\, dz' \\ &\quad - \frac{\epsilon\kappa^2 Z J_1(Z) Z_h K_1(-iZ_h)}{kU_l^2} - \frac{i\epsilon^2\kappa^2 B_1 Z K_1(-iZ)}{U_l}, \end{aligned} \tag{3.151}$$

and for $z > h$

$$\begin{aligned} w^{(\mathrm{UVA})} &= C_o e^{-kz} + D_o e^{kz} + \int_{z_o}^{h} \frac{\cosh k(z-z')}{U_g(z')}\, dz' \\ &\quad - \frac{\epsilon\kappa^2 Z K_1(-iZ) Z_h J_1(Z_h)}{kU_l^2} - \frac{i\epsilon^2\kappa^2 B_1 Z K_1(-iZ)}{U_l}. \end{aligned} \tag{3.152}$$

The streamwise perturbation velocity is obtained by continuity. For $z < h$

$$\begin{aligned} u^{(\mathrm{UVA})} &= -iC_o e^{-kz} + iD_o e^{kz} + \int_{z_o}^{z} \frac{i\sinh k(z-z')}{U_g(z')}\, dz' + \frac{i}{kU_g(z)} \\ &\quad - \frac{J_o(Z) Z_h K_1(-iZ_h)}{kU_l} + \epsilon B_1 K_o(-iZ), \end{aligned} \tag{3.153}$$

and for $z > h$

$$\begin{aligned} u^{(\mathrm{UVA})} &= -iC_o e^{-kz} + iD_o e^{kz} + \int_{z_o}^{h} \frac{i\sinh k(z-z')}{U_g(z')}\, dz' \\ &\quad - \frac{iK_o(-iZ) Z_h J_1(Z_h)}{kU_l} + \epsilon B_1 K_o(-iZ). \end{aligned} \tag{3.154}$$

(3.153) and (3.154) show that the naive solution for $u^{(\mathrm{UVA})}$ is discontinuous at $z = h$ because the jump in the inviscid response terms, $i/(kU_g(h))$, is not cancelled exactly by the jump in the stress gradient terms, $-i/(kU_l)$. These terms *do* cancel each other under the conditions of the small wavenumber analysis, because then h lies well within the inner region and so $U_g(h) = U_l$, given the definition of $U_g(z)$ in §3.5.9; in the large wavenumber case, however, we have $h \gg l$ and $U_g(h) > U_l$.

Let us compare (3.151)–(3.154) with the solutions obtained for the five layers of the large wavenumber analysis in §§3.6.2–3.6.4. The IML solution for leading order pressure (3.127) shows that the first three terms of (3.153) are $-p(z)/U(z)$, local pressure divided by incident velocity. This tends at the bottom of the IML to $-p_o/U_l$, where p_o is the constant SSL pressure. In the SSL, therefore, noting that $U_g(z) \approx U_l$ and that $J_o(Z)K_1(-iZ_h)$ is exponentially small because $z \ll h$, (3.153) becomes identical to the large k SSL solution (3.121). In the IML, $J_o(Z)K_1(-iZ_h)$ is still exponentially small because $z \ll h$, but now $K_o(-iZ)$ is also small because $z \gg l$. Hence all the turbulent stress terms of (3.153) become negligible and the surviving inviscid response terms are plainly identical to the large k IML solution (3.126).

In the $z < h$ half of the RL, z is now close enough to h for $J_o(Z)K_1(-iZ_h)$ to become important, while $K_o(-iZ)$ remains negligible. The first three terms of (3.153) now give $-p_h/U_h$, where p_h and U_h are the constant pressure and incident velocity for the rooftop layer. Therefore the naive solution (3.153) has exactly the same form as the large k RL solution (3.139), except that the large k RL solution uses the local value of incident velocity, U_h, while the naive solution uses the value U_l from far below at $z \approx l$. This applies both to explicit appearances of U_l or U_h in the solutions and to the use of U_l or U_h in the definition of the Bessel function coordinates Z and Y. Exactly the same is true in the $z > h$ half of the RL: the naive solution and the large k solution (3.140) have identical forms but use different values for the incident velocity.

3.6.6 A uniform approximation for all wavenumbers

This detailed comparison shows that we can in fact obtain a uniformly valid approximation for all wavenumbers by means of a simple modification to the small wavenumber solutions (3.151)–(3.154): the SSL incident velocity U_l is replaced wherever it occurs by the blend velocity $U_g(z)$. The definition of Bessel function coordinate Z becomes

$$Z \equiv e^{3i\pi/4}\sqrt{\frac{2U_g(z)kz}{\epsilon\kappa^2}} \qquad (3.155)$$

and explicit occurrences of U_l are also replaced by $U_g(z)$. When, as in the small wavenumber analysis, turbulent stresses are important only within the inner region, this replacement has no effect, since $U_g(z) \approx U_l$ in the inner region. When turbulent stresses become important outside the inner region, for example if there is a strong force gradient around $z = h \gg l$, the replacement modifies the small wavenumber solutions such that they become identical to the detailed solutions from a large wavenumber analysis.

Two characteristics of this simple modification should be noted. Firstly, its effect is similar to the effect in §3.5.8 of incorporating the (U) correction into the original SSL solutions. The replacement of a fixed characteristic velocity U_l by a varying velocity $U_g(z)$ might be justified in general terms by arguing that the perturbations in the SSL vary much more quickly than the incident velocity profile $U(z)$ and hence that any errors introduced by the replacement will be small. This explains why the (U) correction, which allows for the incident velocity profile being $U(z)$ rather than U_l, takes the form it does. The same argument is implicit in the IML solution, since $U(z)$ does not require approximation there.

Secondly, the modification makes no direct reference to the height h whence the problems arise. This is a very important feature. It justifies our use of the canonical force distribution (3.120) and shows that the same modification applies equally well to force distributions which may include strong force gradients at a number of different heights.

3.7 Sample results

To illustrate the analysis we present small and large wavenumber responses to a distributed force whose drag coefficient is constant up to the height $h^* = 60\text{mm}$ and then vanishes; consequently the force in $z_o^* \leq z^* \leq h^*$ varies as the square of incident velocity. The incident velocity is logarithmic with friction velocity $u_* = 0.64\text{ms}^{-1}$ and roughness height $z_o^* = 0.4\text{mm}$. For a single wavenumber k, real and imaginary parts of the results for a given quantity ϕ show the progression of that quantity in passing

through a sinusoidally varying force distribution with wavenumber k: $\mathrm{Re}\{\phi\}$ is the actual profile at points where the resistance is a maximum and $\mathrm{Im}\{\phi\}$ is the actual profile at points where the resistance is zero and increasing; see figure 3.3.

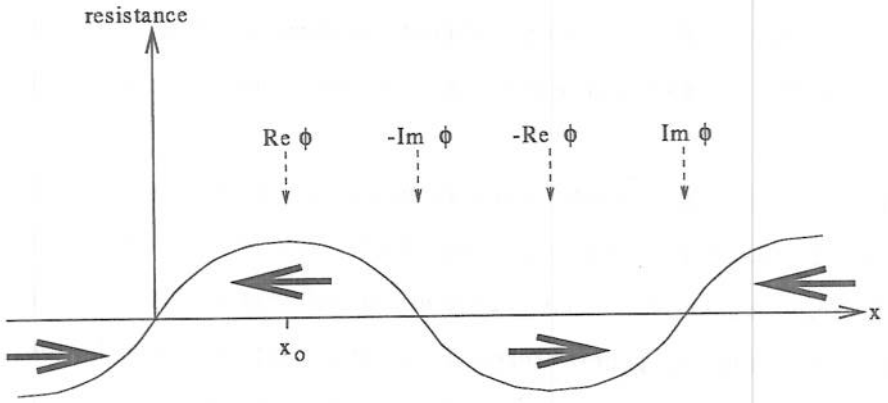

Figure 3.3: Real and imaginary parts of a solution represent the actual profile at different stages of passage through a sinusoidally varying resistance. The general profile at streamwise location x is $\mathrm{Re}\{\phi\}\cos k(x-x_o) - \mathrm{Im}\{\phi\}\sin k(x-x_o)$, where x_o is a location of maximum resistance.

3.7.1 Matching between the inner and outer regions

Figures 3.4 and 3.5 illustrate small and large wavenumber matching respectively. Each figure shows real and imaginary parts of the vertical velocity w as given by the inner region solution (3.88, 3.89), the outer region solution (3.99) and the uniformly valid approximation (3.119). In figure 3.4 $l^* = 0.65$m so that $l^* \gg h^*$ and significant force gradients are contained within the inner region. In figure 3.5 $l^* = 0.035$m so that $l^* \ll h^*$: the rooftop layer around h^* is noticeable as a region where the gradient of w varies rapidly. In both cases matching between inner and outer regions is good, such that the uniformly valid approximation asymptotes correctly to the inner and outer region solutions for $z \ll l$ and $z \gg l$ and makes a smooth transition between them for $z = O(l)$.

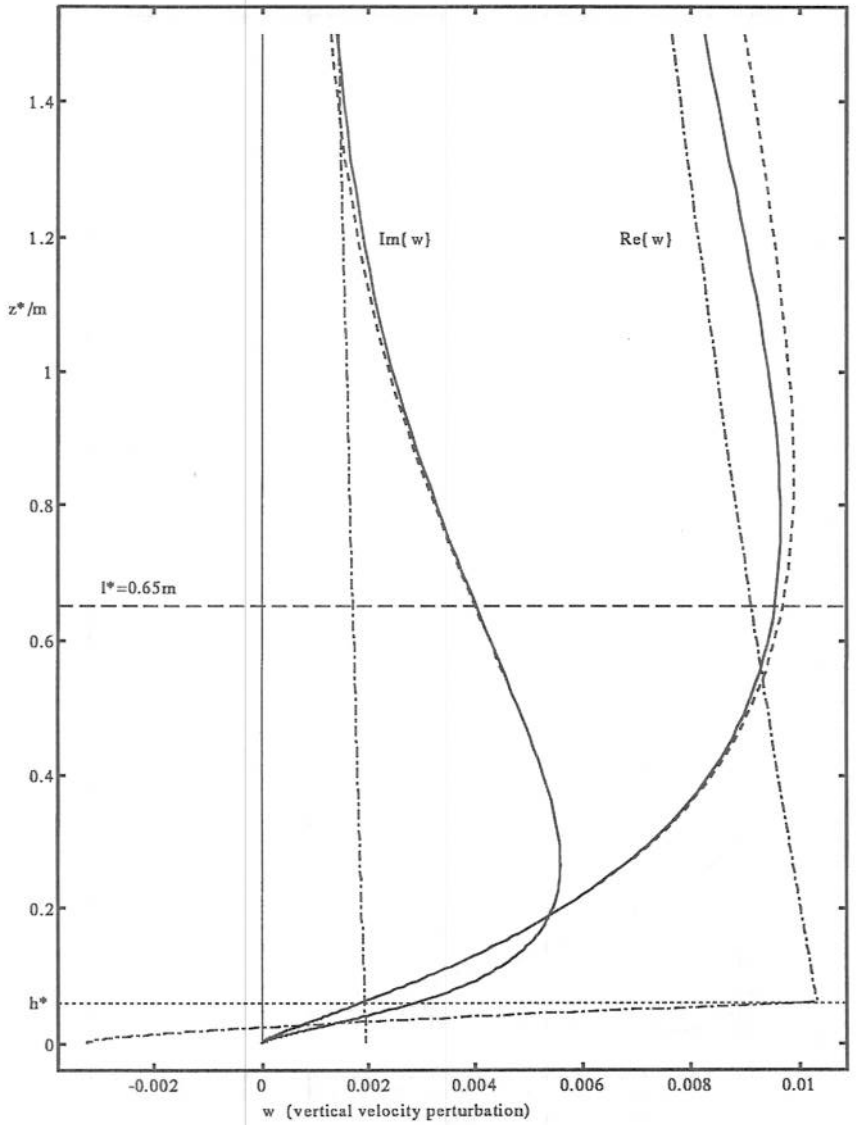

Figure 3.4: Illustration of inner/outer region matching at small wavenumbers, showing real (to the right) and imaginary (to the left) parts of the vertical velocity perturbation w. Single dashed lines show the inner region solution; double dashed lines show the outer region solution; solid lines show the uniformly valid approximation.

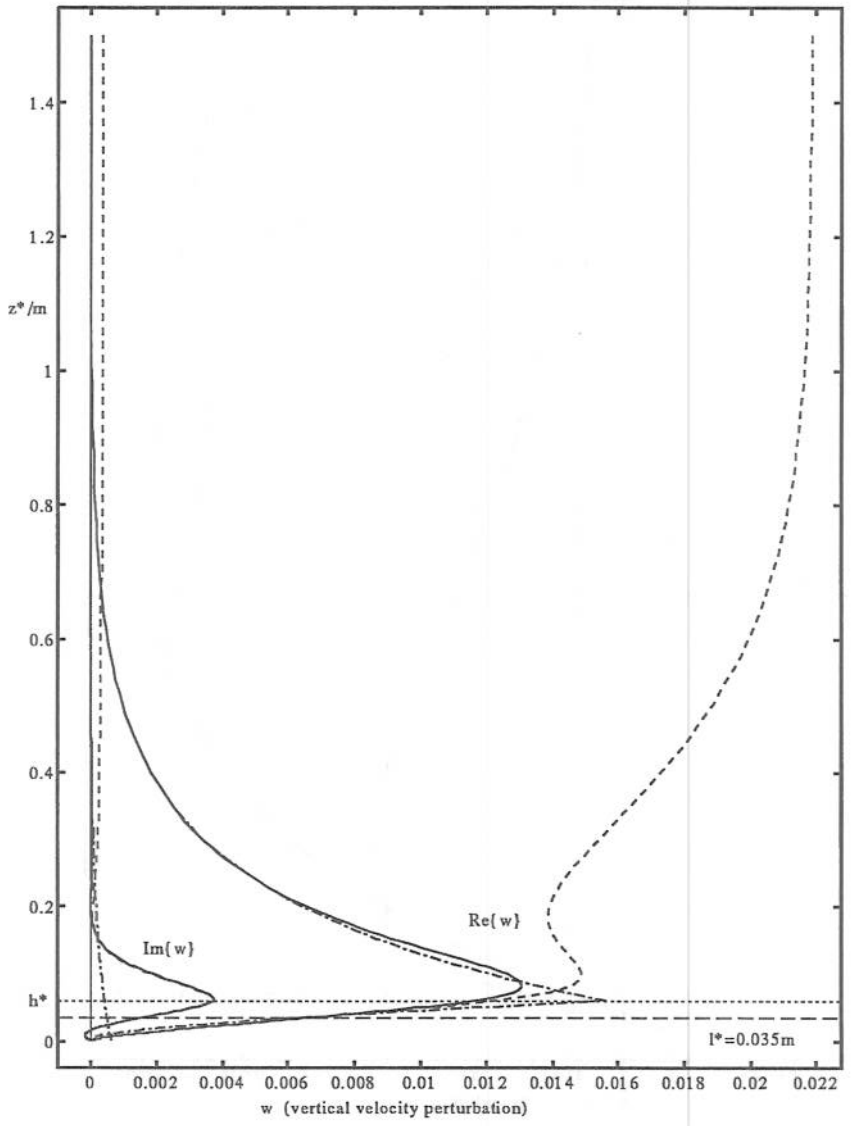

Figure 3.5: Illustration of inner/outer region matching at large wavenumbers, showing real (to the right) and imaginary (to the left) parts of the vertical velocity perturbation w. Single dashed lines show the inner region solution; double dashed lines show the outer region solution; solid lines show the uniformly valid approximation.

3.7.2 Small and large wavenumber responses

Figures 3.6–3.9 show the uniformly valid perturbation velocities, pressure and turbulent shear stress that comprise the response to a slowly varying force distribution. Dashed lines show the effect of including the $O(\epsilon)$ incident velocity shear correction. Notice how the spread of streamwise velocity defect increases as the flow moves downstream from the location of maximum resistance (profile = $\mathrm{Re}\, u$) to that of zero resistance (profile = $-\mathrm{Im}\, u$), showing the diffusive effects of turbulent stress. Correspondingly, $-\mathrm{Im}\, \tau$ shows a constant stress layer above $z^* = h^*$ which is not evident in the $\mathrm{Re}\, \tau$ profile further upstream.

Figures 3.10–3.13 present similar results for a rapidly varying force distribution. Here the flow is quasi-inviscid, except for turbulent stress effects which meet the no-slip condition at the ground and smooth out sharp gradients in the rooftop layer. Hence the streamwise velocity is largely confined to $z_o^* \leq z^* \leq h^*$, turbulent stress is small except near the ground and near $z^* = h^*$, and the pressure profile is like that associated with outflow from a source.

The effect of the incident velocity shear correction is generally to increase the magnitude of the streamwise velocity perturbations. In $z^* < h^*$ the *deceleration* due to resistance is increased by this correction, while in $z^* > h^*$ at large wavenumbers the *acceleration* over the top of the distribution is increased. Similarly, in turbulent flow over a low hill the incident shear correction increases the speed-up over the crest of the hill.

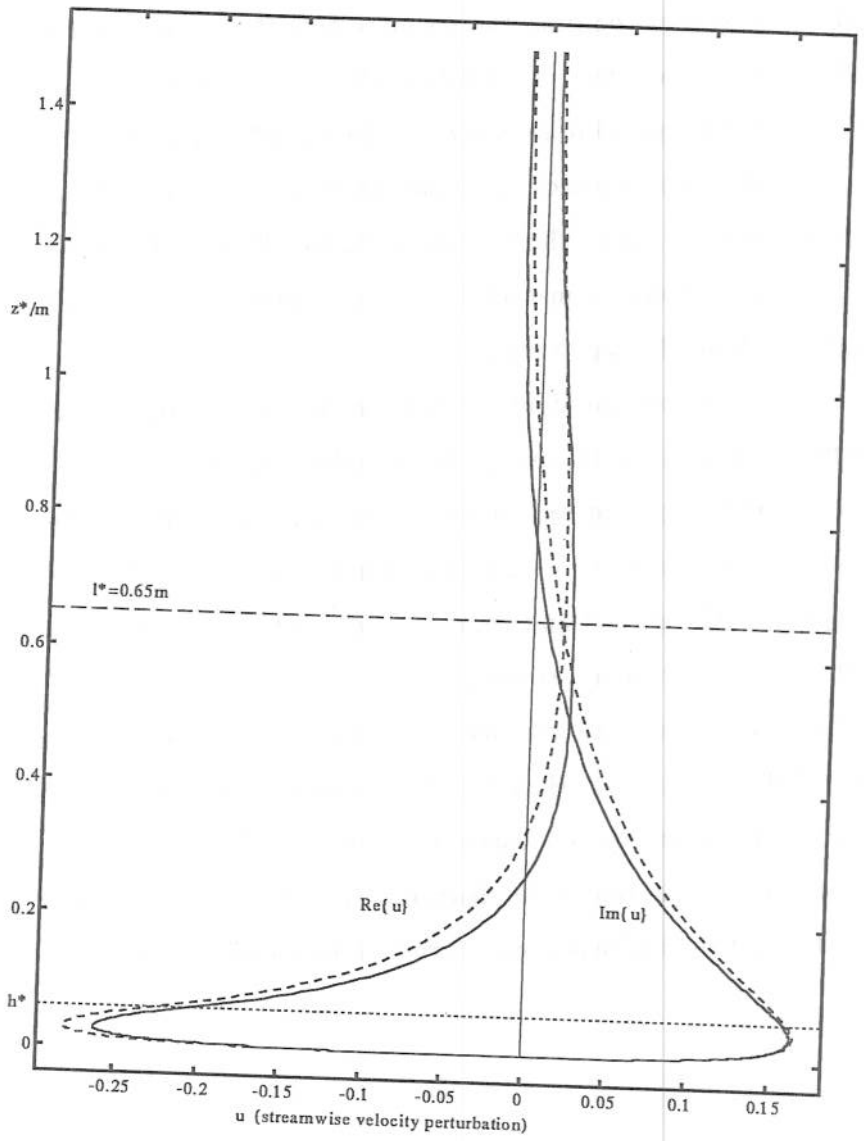

Figure 3.6: Perturbation streamwise velocity at small wavenumbers: real part to the left, imaginary part to the right. Dashed lines show the effect of including the incident velocity shear correction.

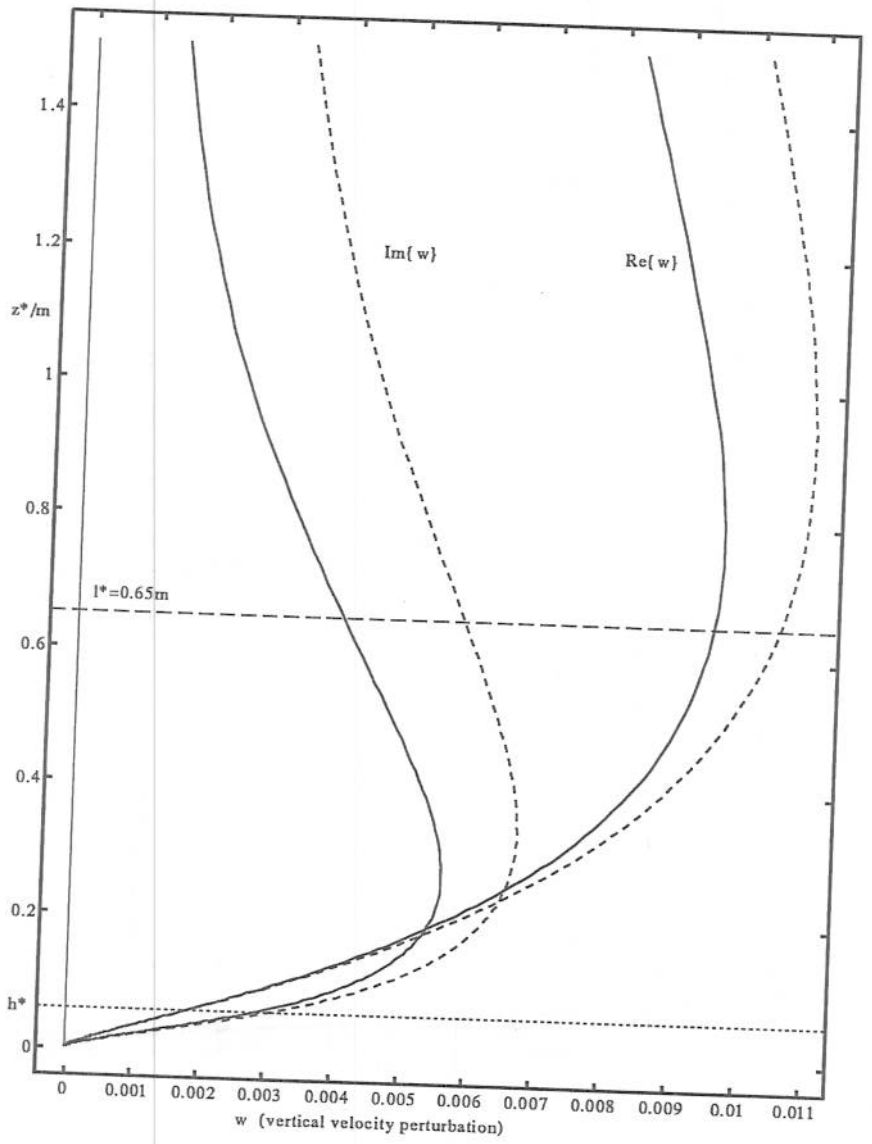

Figure 3.7: Perturbation vertical velocity at small wavenumbers: real part to the right, imaginary part to the left. Dashed lines show the effect of including the incident velocity shear correction.

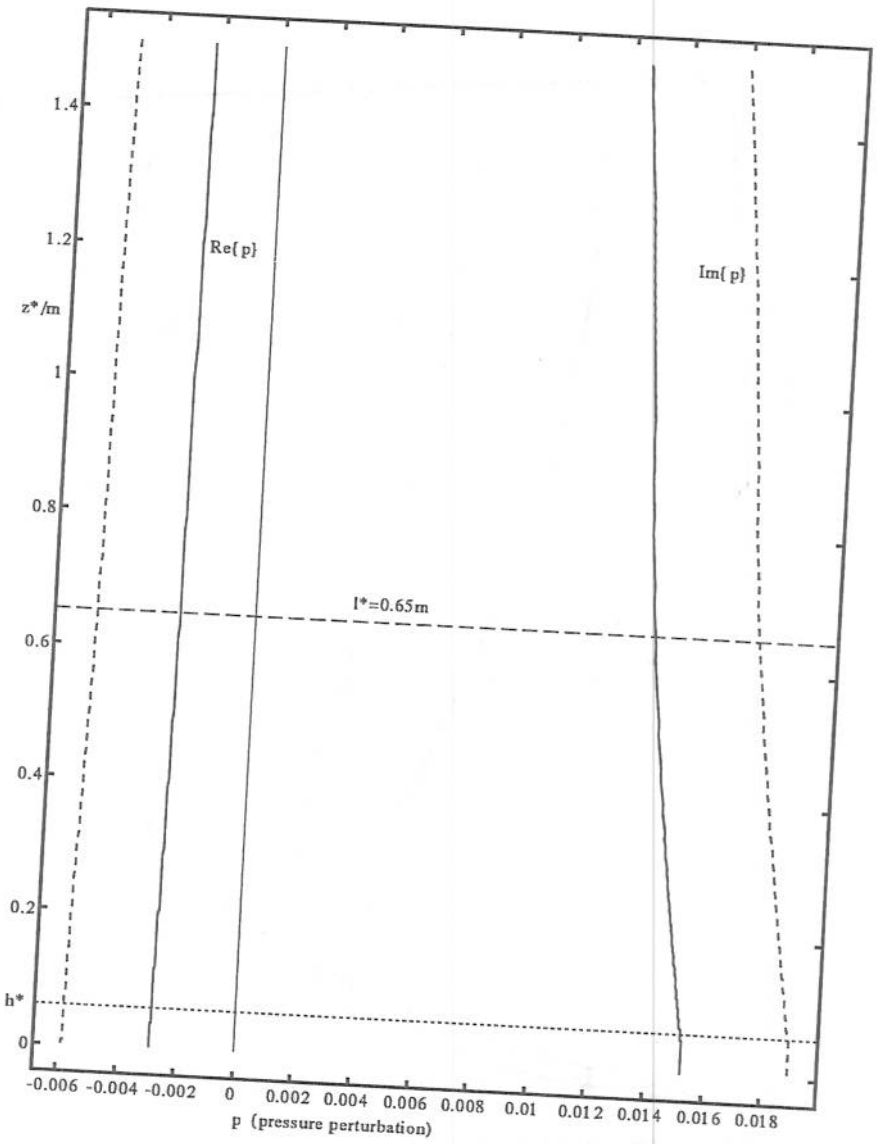

Figure 3.8: Perturbation pressure at small wavenumbers: real part to the left, imaginary part to the right. Dashed lines show the effect of including the incident velocity shear correction.

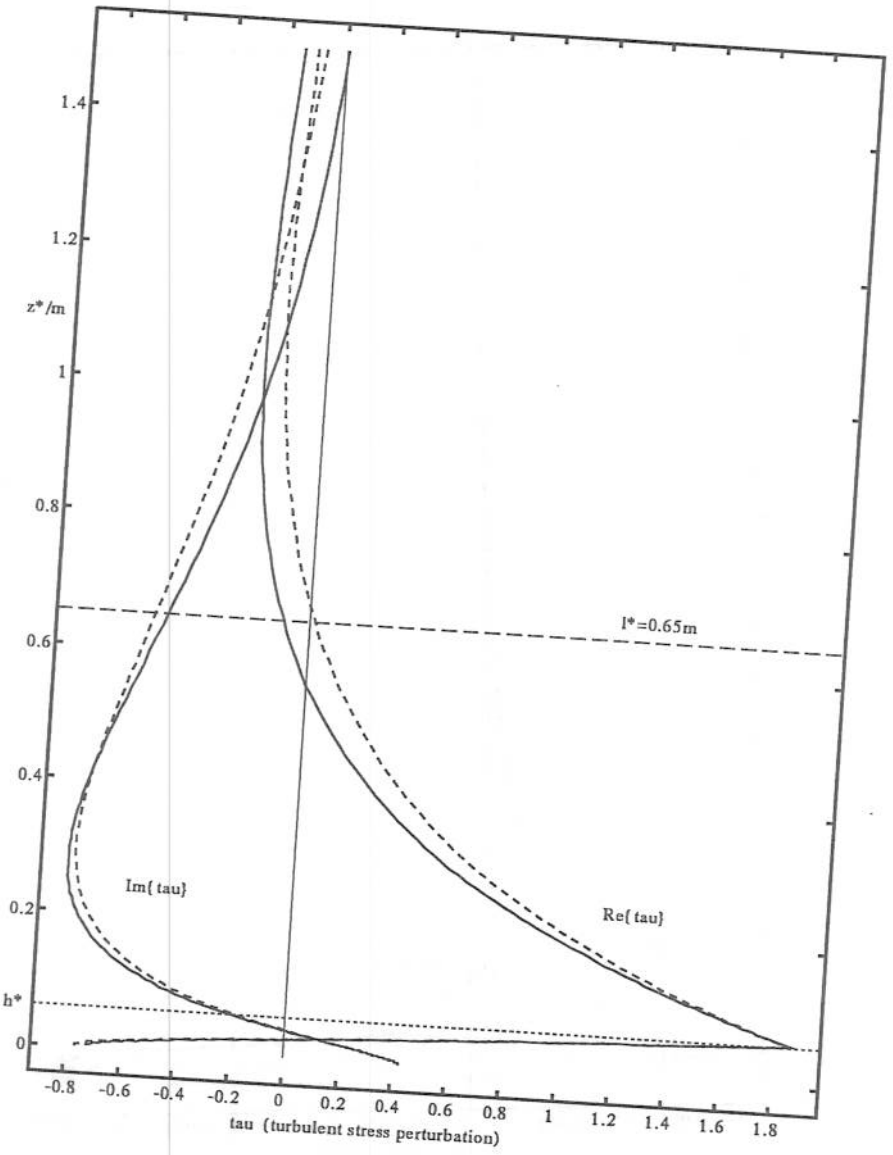

Figure 3.9: Perturbation shear stress at small wavenumbers: real part to the right, imaginary part to the left. Dashed lines show the effect of including the incident velocity shear correction.

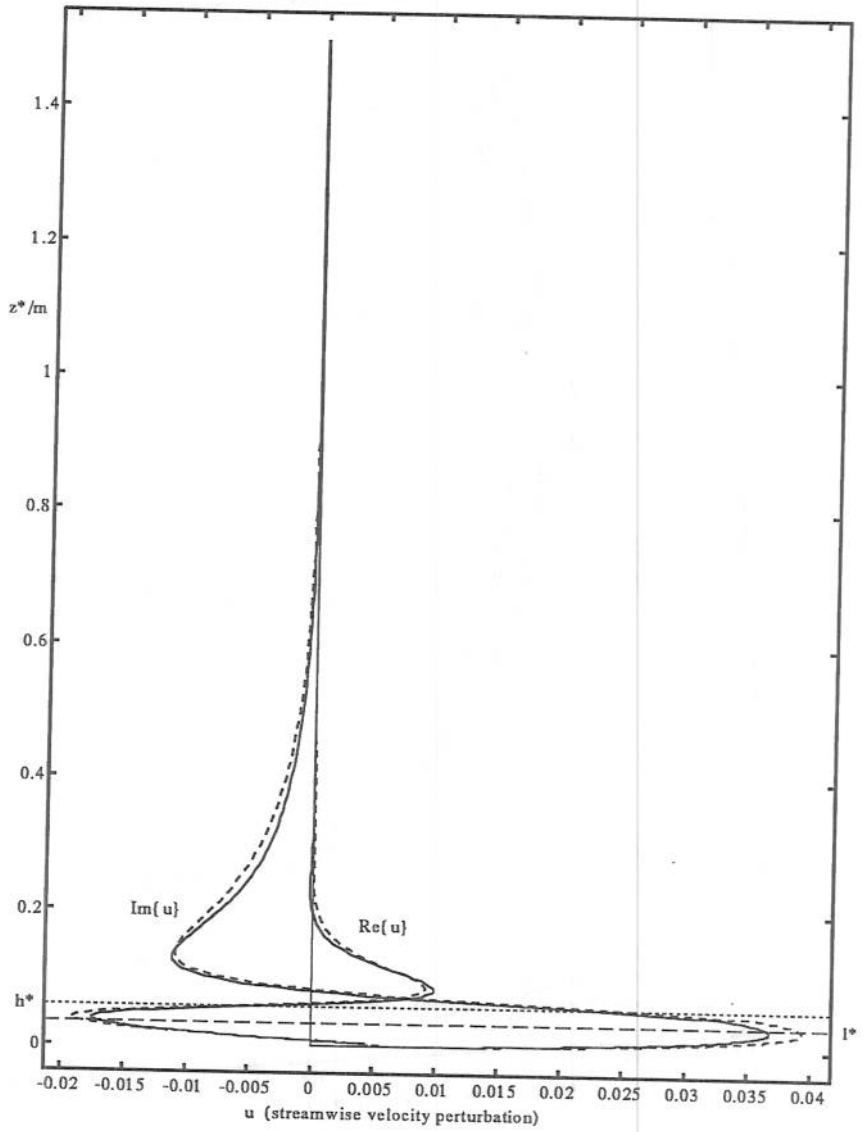

Figure 3.10: Perturbation streamwise velocity at large wavenumbers: real part to the left in $z^* < h^*$, imaginary part to the right. Dashed lines show the effect of including the incident velocity shear correction.

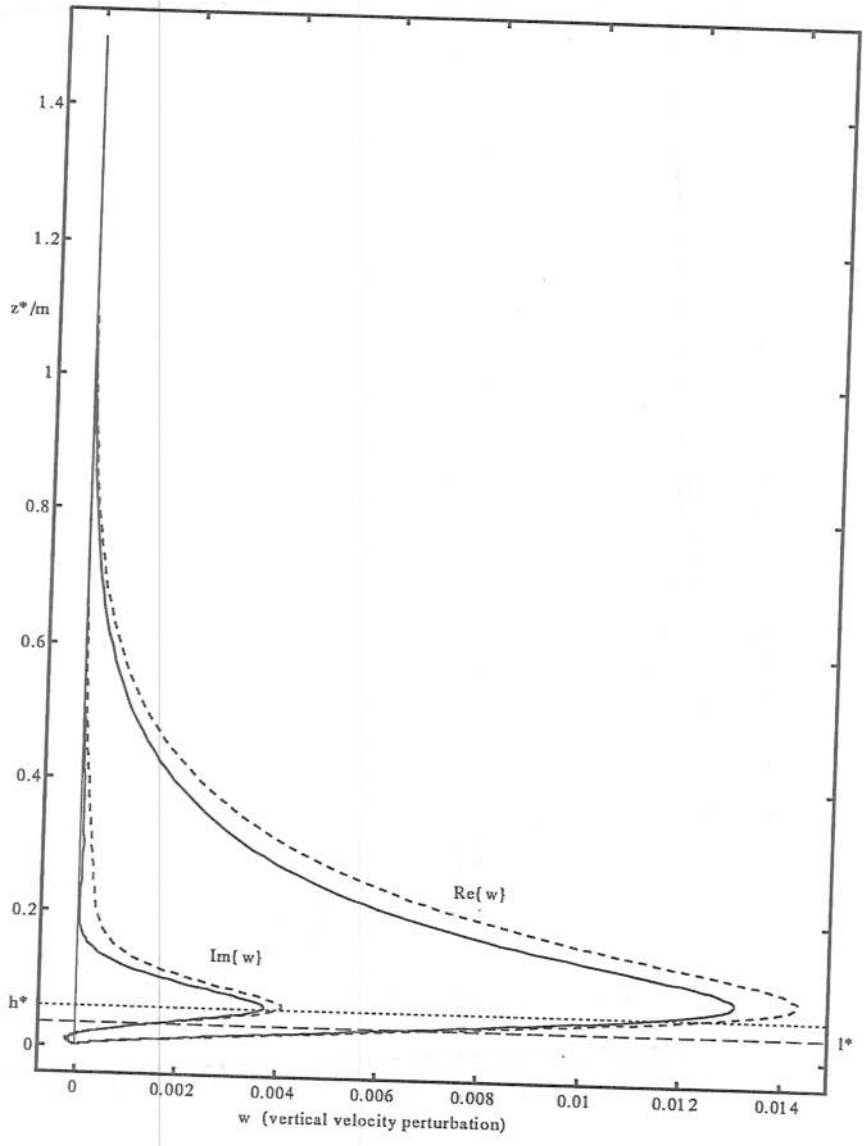

Figure 3.11: Perturbation vertical velocity at large wavenumbers: real part to the right, imaginary part to the left. Dashed lines show the effect of including the incident velocity shear correction.

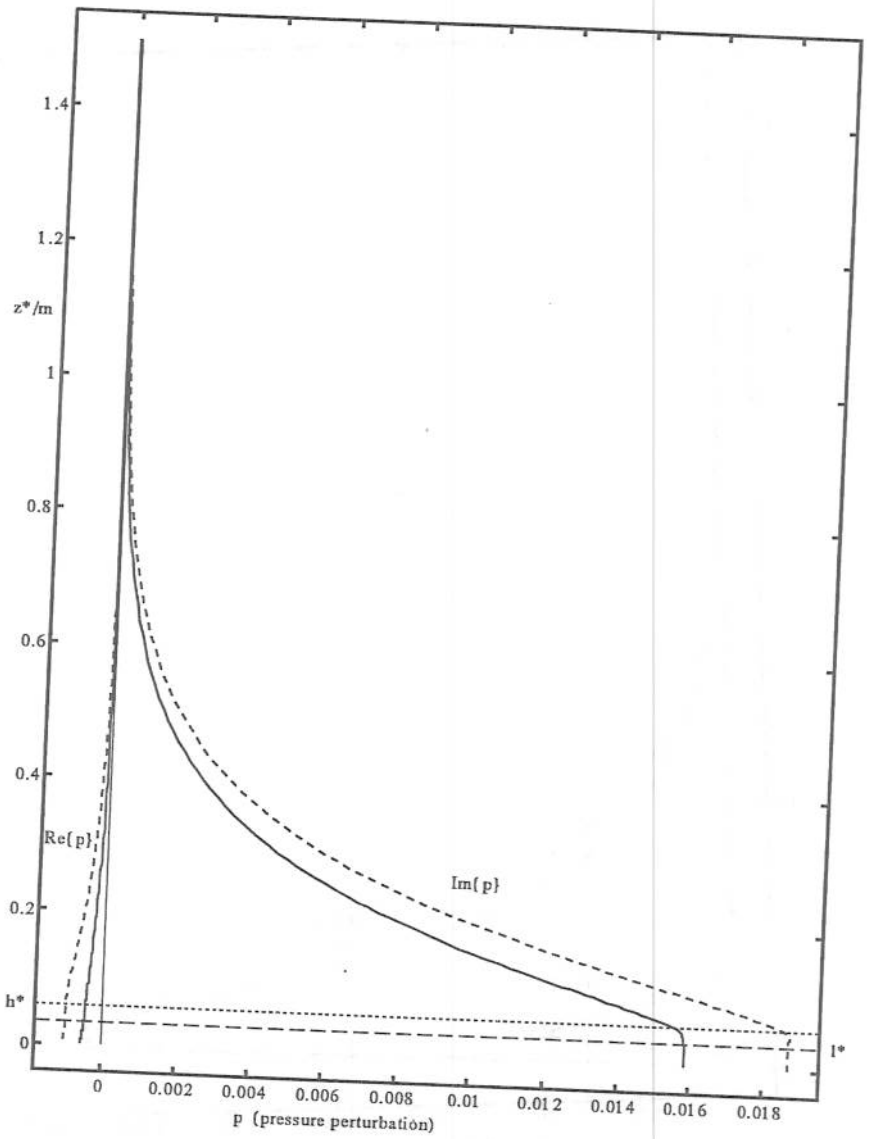

Figure 3.12: Perturbation pressure at large wavenumbers: real part to the left, imaginary part to the right. Dashed lines show the effect of including the incident velocity shear correction.

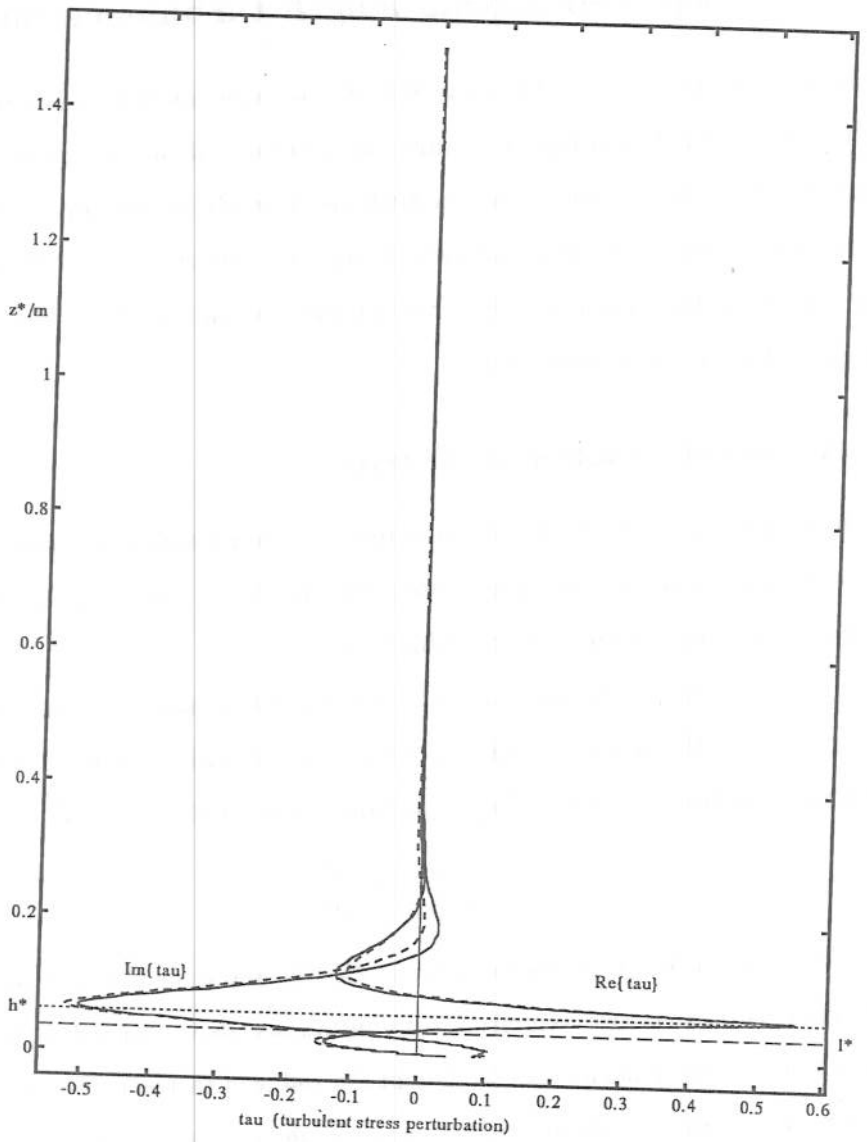

Figure 3.13: Perturbation shear stress at large wavenumbers: real part to the right, imaginary part to the left. Dashed lines show the effect of including the incident velocity shear correction.

3.8 The displaced mixing length turbulence model

According to the discussion of §3.1, the SML turbulence model becomes invalid if mean flow changes are strong enough to change the structure of the turbulence from that in the incident flow. In this section a new turbulence model is developed that takes into account such strong effects of mean flow changes on the turbulence. This "displaced" mixing length model is then used in a new analysis of the flow field perturbations due to a region of distributed resistance.

3.8.1 Effects of a rooftop shear layer

When the buildings in a group have approximately equal heights, the force distribution used to model them has a well-defined, coherent "rooftop," where the distributed force decreases rapidly from its maximum value to zero.

The inviscid response to such a force distribution (chapter 2) includes a strong shear layer around the rooftop height, in which the vertical gradient of streamwise velocity increases following the flow in proportion to the local distributed force gradient:

$$\frac{\partial}{\partial x}\frac{\partial u}{\partial z} \propto \frac{\partial f}{\partial z}. \tag{3.156}$$

In the limit in which the distributed force is discontinuous at the rooftop height, the inviscid response streamwise velocity is discontinuous also. According to the model of §§3.5–3.6, the rooftop shear layer's strength is reduced in the turbulent flow by the mixing action of turbulent shear stresses, but the shear layer is still strong enough to dominate flow around the rooftop height.

Such strong shear layers can have a significant effect upon the turbulence above and below them. Two quite different mechanisms both suggest that a strong shear layer acts to block turbulent motions across it. Firstly there is the dissipation mechanism described by Hunt *et al.* (1988b) and Belcher *et al.* (1991a, 1991b) and illustrated schematically in figure 3.14. Turbulent eddies that enter the shear layer are stretched out by the shear flow to an elongated shape. Hence vertical velocity gradients are amplified and turbulent dissipation increases. The shear flow inhibits motion of tur-

Figure 3.14: The effect of a strong shear layer in increasing turbulent dissipation.

bulent eddies across the shear layer and leads to weak correlation between the flows above and below the shear layer. The increased turbulent dissipation within the shear layer can be modelled as a reduction in the turbulent mixing/dissipation length scale; hence the above authors' shear-dependent mixing length model,

$$\lambda_m^{-1} = \frac{A_B}{\kappa z} + \frac{A_s}{u_*}\frac{\partial U}{\partial z}, \tag{3.157}$$

known as the Shear Blocking Mixing Length model.

Secondly, recent studies by Craik (1991) and Hunt (unpublished) investigate a purely inviscid effect of strong shear layers, illustrated schematically in figure 3.15. Inviscid analysis of a travelling linear disturbance above a vortex sheet shows that there is no induced disturbance *below* the vortex sheet if the phase speed of the disturbance equals the advection velocity U. Extrapolation of this result to the case of turbulent eddies advected by the mean flow above a strong shear layer again suggests that a shear layer acts to block turbulent motions across it and hence provides a reference level for the turbulence above and below.

The effects of these blocking mechanisms will now be investigated in the context of flow through a group of buildings.

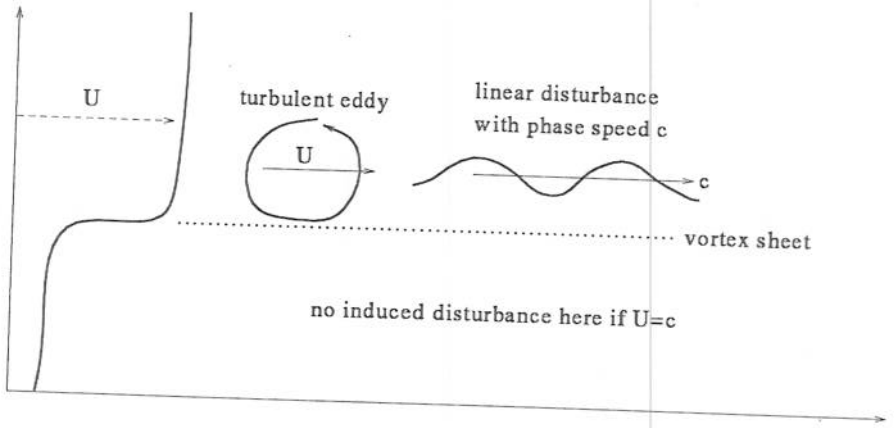

Figure 3.15: The effect of a travelling linear disturbance above a vortex sheet.

3.8.2 The shear layer produced by a group of buildings

There is good reason to suspect that the distributed force model actually underestimates the strength of the rooftop shear layer. To obtain a physical picture of how shear layers are created, it is useful to step back from the distributed resistance model and consider explicitly a group of obstacles in a turbulent boundary layer (figure 3.16). Vorticity created along an obstacle's upper surface is shed from the trailing edge of that surface to form a thin shear layer (cf. the experiments on single surface-mounted obstacles by Castro & Robins 1977). This vorticity is advected downstream towards the next obstacle and also diffuses vertically, so that the shear layer spreads. The shear layer spreads more down towards the ground than upwards because average wind speeds between the obstacles are much lower than those just above them, and because the shed vortices are deflected downwards by their own induced velocity field. Immediately above each building's roof, turbulent eddies are blocked by the roof surface and so the length scale of the turbulence should scale on height above the roof. Hence turbulent mixing here is much less vigorous than that in the SML model used in §§3.2–3.7 and the rooftop surface shear layers are much more concentrated in reality than in the model. Therefore the rooftop shear layer as a whole, comprising boundary layers on building roofs and free shear layers between buildings, is likely to be rather

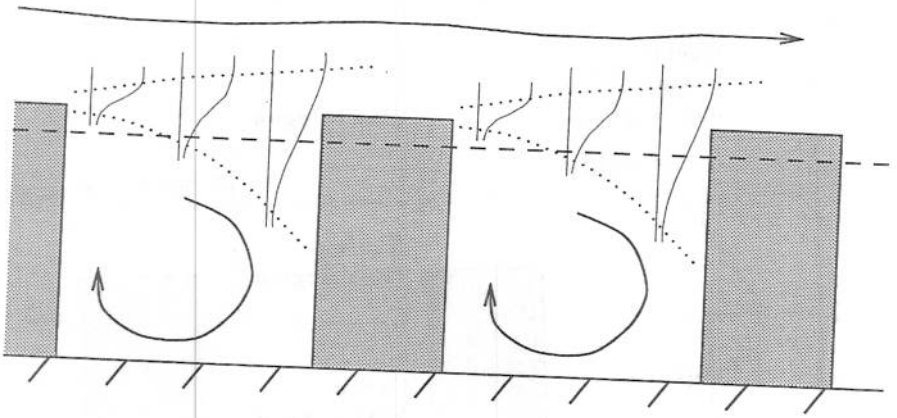

Figure 3.16: The spreading of shear layers shed from obstacle roofs. The dotted lines indicate the approximate extent of the spreading shear layer; the dashed line shows its horizontally averaged mean height.

stronger than that in the SML distributed force analysis.

Clearly a new turbulence model is required to take account of the effects of a concentrated rooftop shear layer. The new formulation is an attempt to account for some of the single obstacle-scale influences on the flow, particularly in the vicinity of the rooftop, that were lost during the horizontal averaging operation.

3.8.3 The displaced mixing length model

The proposed new model is illustrated schematically in figure 3.17. The principal effect of a concentrated shear layer is to inhibit turbulent motions across it: the turbulent length scale within the shear layer is reduced and turbulent eddies above the shear layer appear to be blocked as though by a solid surface at a reference height within or just below the shear layer. This behaviour can be modelled by defining a displacement height d and a roughness height z_o' for the turbulent mixing within and above the shear layer. The displacement height d is the reference level with respect to which eddies above the shear layer appear to be blocked. The roughness height z_o' parameterises the turbulent mixing and dissipation within the shear layer: $\kappa z_o'$ is

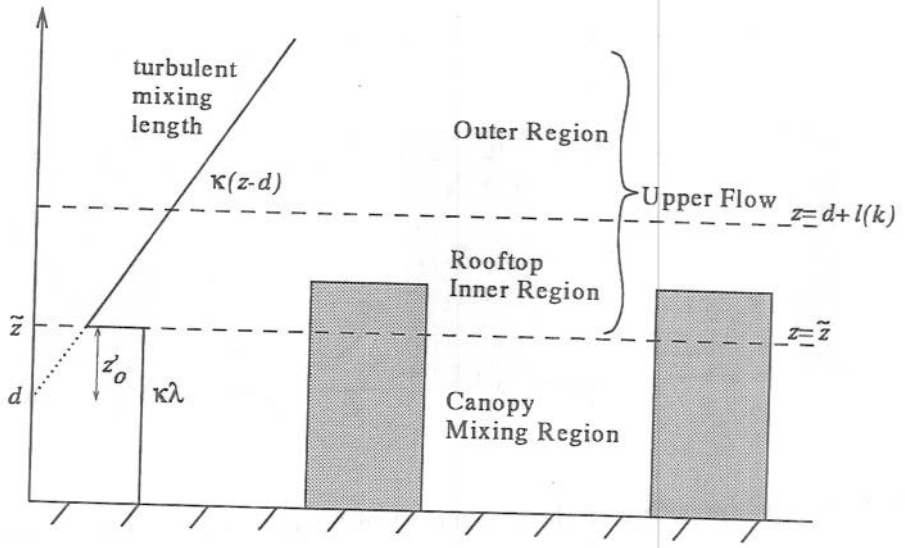

Figure 3.17: Flow structure for the displaced mixing length model.

the minimum value of the turbulent length scale there. Note, following Panofsky & Dutton (1984, chapter 6), how the roughness height is primarily a dynamical measure of turbulent mixing, not a geometrical measure of roughness elements on a surface, and so may be used to parameterise turbulent mixing at any interface whether or not roughness elements are present.

In the "canopy mixing region" below $z = \tilde{z}$ a new model is used. The field and wind tunnel experiments of Davidson *et al.* (1995a,b), on flow through an array of cubical obstacles, showed that the turbulence length scale within the obstacle canopy was much smaller than that in the incident flow. This suggests that the turbulence between obstacles is dominated by high intensity small scale turbulence generated by vortices shed from individual obstacles. In many canopies, where horizontal obstacle dimensions are smaller than obstacle heights, the resultant turbulent mixing will be (i) on a smaller length scale than the blocking length scale κz and (ii) uniform over most of the depth of the canopy (assuming the horizontal obstacle dimensions are approximately constant with height). Thus the turbulence in $z_o < z < \tilde{z}$ is modelled here by a constant eddy viscosity. The laminar viscous analysis of §2.9, which uses a

constant eddy viscosity, is therefore appropriate for the canopy region $z_o < z < \tilde{z}$.

Once general solutions for the upper flow and the canopy mixing region have been obtained, they are matched together at $z = \tilde{z}$ by requiring streamwise velocity, vertical velocity, pressure and shear stress to be continuous. If the turbulent mixing length is discontinuous, as shown in figure 3.17, it follows that the streamwise velocity gradient will be discontinuous also.

3.8.4 Interpretation of the model parameters

According to the discussion of §3.8.2, the new model parameters should be related to the geometry of the rooftop shear layer. The distortion of turbulent eddies illustrated in figure 3.16 suggests that z_o' is of the order of the shear layer thickness and that the sum $\tilde{z} \equiv d + z_o'$ is the mean height of the shear layer. Hence d and z_o' are determined by the distribution of obstacles within a group, in particular by obstacle density. In a dense array with little space for the shear layer to spread between obstacles, d and z_o' are determined mainly by the boundary layer on the obstacle roofs, *i.e.* by the obstacles' height and the surface roughness of their roofs. Conversely, in a sparse array where the shear layer spreads down to the ground between obstacles, $d \ll h$ and z_o' is determined mainly by the roughness of the ground.

Note that the roughness height z_o' used here to describe turbulent mixing within the shear layer is not equivalent to the roughness height z_1 that is obtained by fitting a logarithmic profile,

$$\hat{u}^*(z) = \frac{u_* + \Delta u_*}{\kappa} \ln \frac{z - d_1}{z_1}, \tag{3.158}$$

to the flow above the buildings. The connection between z_o' and z_1 will be examined in chapter 5. The parameter d, on the other hand, can be identified with the displacement height d_1 in (3.158). The question therefore arises: is the notion of d as some measure of a spreading shear layer compatible with other interpretations of the displacement height?

Thom (1971) observed experimentally that the level d_o at which the drag on a rough surface appears to act coincided, to within experimental error, with the dis-

placement height d_1 obtained by fitting the model profile (3.158) to the flow above the surface. That is, he found that

$$d_1 = d_o \equiv \mu_o/\tau_o, \tag{3.159}$$

where μ_o is the streamwise moment per unit area about the surface and τ_o is the streamwise force per unit area. Jackson (1981) showed that the idea of a reference level or displacement height, at or near a rough surface, is implicit in the usual derivation, using dimensional analysis, of the logarithmic profile; otherwise the logarithmic law would not be invariant under a translation of the vertical coordinate system. Following Thom's observation, Jackson then proposed (3.159) as a reliable model for predicting the displacement height over any rough surface. Neither Thom nor Jackson, however, suggested a physical mechanism to explain why the displacement should obey (3.159).

The strong shear layer mechanism discussed in §§3.8.1–3.8.2 could be the missing link. The shear layer determines d by blocking turbulent motions across it, hence providing a reference level for the turbulent eddies above; the reference level then appears as a displacement height in the observed velocity profile (3.158). The shear layer also characterises the flow field that impinges upon downstream obstacles and thus controls the force and moment that act upon the surface. Therefore a relationship such as (3.159) between displacement height and forces on the surface is to be expected.

3.8.5 Velocity profile calculation in $z < \tilde{z}$

The canopy mixing region (CMR) flow is calculated using the analysis of §2.9 with $Re = U_c/(2\epsilon\kappa^2\lambda)$, where $U_c \equiv U(\tilde{z})$ is the canopy velocity scale and λ is the constant mixing length. From (2.29)–(2.31), the general solution for the perturbation streamfunction ψ is expressed in terms of two complementary functions $q_1(k,z)$ and $q_2(k,z)$ and a Green's function $g(k,z;z')$:

$$\psi(k,z) = s_1 q_1(k,z) + s_2 q_2(k,z) + \frac{Re}{U_c}\int_{z_o}^{z} \frac{\partial f}{\partial z}(z') g(k,z;z')\, dz',$$

where

$$q_1(k,z) \equiv \sinh\alpha(z-z_o) - \frac{\alpha}{\beta}\sinh\beta(z-z_o),$$

$$q_2(k,z) \equiv \cosh\alpha(z-z_o) - \cosh\beta(z-z_o),$$
$$\text{and} \quad g(k,z;z') \equiv \frac{\sinh\alpha(z-z')}{\alpha(\alpha^2-\beta^2)} - \frac{\sinh\beta(z-z')}{\beta(\alpha^2-\beta^2)}.$$

Recall from §2.9 that $\beta = |k|$ and $\alpha^2 = k^2 + ikRe$ such that the real part of α is non-negative. Then the perturbation velocities, pressure and shear stress are given in terms of ψ by

$$u = \frac{\partial\psi}{\partial z}; \tag{3.160}$$
$$w = -ik\psi; \tag{3.161}$$
$$p = \frac{2\epsilon\kappa^2\lambda}{ik}\left(\frac{\partial^3}{\partial z^3} - k^2\frac{\partial}{\partial z}\right)\psi - U_c\frac{\partial\psi}{\partial z} - \frac{f}{ik}; \tag{3.162}$$
$$\tau = \frac{2\lambda}{\epsilon}\left(k^2 + \frac{\partial^2}{\partial z^2}\right)\psi. \tag{3.163}$$

These profiles depend implicitly on the constants s_1 and s_2 which are to be determined by matching with the upper part of the flow. Thus at $z = \tilde{z}$ we have

$$\tilde{u} = u(\tilde{z};s_1,s_2); \quad \tilde{w} = w(\tilde{z};s_1,s_2); \quad \tilde{p} = p(\tilde{z};s_1,s_2); \quad \tilde{\tau} = \tau(\tilde{z};s_1,s_2),$$

which are all linear functions of s_1 and s_2.

3.8.6 Velocity profile calculation in $z > \tilde{z}$

The upper flow is analysed using the methods developed for the SML analysis in §§3.5–3.6. The main differences are that (i) the flow is displaced upwards by a distance $\tilde{z}-z_o$ and (ii) the lower boundary condition is $\mathbf{u}(\tilde{z}) = (\tilde{u},\tilde{w})$ instead of $\mathbf{u} = 0$. Here we focus on the smaller wavenumber analysis, such that there are no strong force gradients in the outer region of the flow. Large wavenumber results may be obtained by following the approach of §3.6 with appropriate modifications.

Asymptotic structure of the upper flow

The upper limit z_l of the rooftop inner region (RIR) is determined, as in §3.3, by the balance between time scales for advection by the mean flow and for turbulent eddy

adjustment. Taking into account the new reference level d for the turbulent eddies of the upper flow, the time scale balance is

$$\frac{1}{kU^*(z_l)} \approx \frac{z_l - d}{u^*}. \tag{3.164}$$

Therefore the vertical size of the RIR, $l \equiv z_l - d$, satisfies

$$kl \ln \frac{d+l}{z_o} = 1. \tag{3.165}$$

The small parameter ϵ is defined as in §3.3, namely $\epsilon \equiv \ln^{-1}(H/z_o)$. It remains true that $kl = O(\epsilon)$ since $d = O(H)$. The RIR velocity scale is defined by

$$U_l \equiv U(d+l) = \epsilon \ln \frac{d+l}{z_o}, \tag{3.166}$$

so then the incident velocity profile in the RIR may be expressed as

$$U(z) = U_l + \epsilon \ln \frac{z}{d+l}. \tag{3.167}$$

It is not necessary to subdivide the RIR because $U(z)$ is well approximated by U_l throughout the region.

The rooftop inner region

In the upper flow, the turbulent mixing length is $\kappa(z-d)$. Therefore the turbulent stress model becomes

$$\tau = \frac{2(z-d)}{\epsilon} \frac{\partial u}{\partial z}. \tag{3.168}$$

Define the RIR coordinate $\zeta \equiv (z-d)/l$; the governing equations are then

$$ikl(U_l + O(\epsilon))u + \epsilon wl/z + iklp = 2\epsilon\kappa^2(\zeta u')' - lf; \tag{3.169}$$

$$ikl(U_l + O(\epsilon))w + p' = 2ikl\epsilon\kappa^2\zeta u'; \tag{3.170}$$

$$iklu + w' = 0. \tag{3.171}$$

The non-zero vertical velocity at $z = \tilde{z}$ means that the leading order streamwise momentum equation differs slightly from (3.38):

$$iklU_l u_o - 2\epsilon\kappa^2(\zeta u_o')' = -lf - iklp_o - \epsilon\tilde{w}l/z. \tag{3.172}$$

The last term in (3.172) is another manifestation of the $O(\epsilon)$ additional force distribution $\epsilon w/z$ that may be applied to the whole of the upper flow. Putting this term to one side (for later correction), the general solution is

$$\begin{aligned} u_o &= A_o J_o(Z) + B_o K_o(-iZ) - \frac{p_o}{U_l} \\ &\quad + \frac{i}{kU_l}\int_{\tilde{Z}}^{Z} Z' f(z') \left\{ J_o(Z) K_o(-iZ') - J_o(Z') K_o(-iZ) \right\} dZ', \end{aligned} \tag{3.173}$$

where

$$Z \equiv e^{3i\pi/4}\sqrt{\frac{2U_l k(z-d)}{\epsilon\kappa^2}}. \tag{3.174}$$

A_o is determined by the constraint of boundedness as $\zeta \to \infty$:

$$A_o + \frac{i}{kU_l}\int_{\tilde{Z}}^{\infty} Z' f(z') K_o(-iZ') dZ' = 0. \tag{3.175}$$

The three contributions to the first order correction u_1 are determined as shown in §3.5 except that now $f_1^{(\mathrm{U})} \equiv iku_o(U - U_l)/\epsilon$. Then the streamwise velocity boundary condition at $z = \tilde{z}$, namely $u(\tilde{z}) = \tilde{u}$, shows that $B_o = 0$ as before and that

$$A_o J_o(\tilde{Z}) + \epsilon B_1 K_o(-i\tilde{Z}) - \frac{p_o}{U_l} = \tilde{u}. \tag{3.176}$$

Differentiation of the streamwise velocities u_o and $u_1^{(\mathrm{cf})}$ gives the shear stresses:

$$\begin{aligned} \tau_{-1} &= -A_o Z J_1(Z) \\ &\quad - \frac{iZ}{kU_l}\int_{\tilde{Z}}^{Z} Z' f(z') \left\{ J_1(Z) K_o(-iZ') + iJ_o(Z') K_1(-iZ) \right\} dZ'; \end{aligned} \tag{3.177}$$

$$\tau_o^{(\mathrm{cf})} = iB_1 Z K_1(-iZ). \tag{3.178}$$

The vertical velocity is $w = \tilde{w} + \epsilon w_1 + \epsilon^2 w_2^{(\mathrm{cf})} + \ldots$, where

$$\epsilon U_l w_1 = ikp_o(z - \tilde{z}) + \int_{\tilde{z}}^{z} f(z')\, dz' - \epsilon\kappa^2(\tau_{-1} + A_o \tilde{Z} J_1(\tilde{Z})); \tag{3.179}$$

$$\epsilon U_l w_2^{(\mathrm{cf})} = -\epsilon\kappa^2(\tau_o^{(\mathrm{cf})} - iB_1 \tilde{Z} K_1(-i\tilde{Z})). \tag{3.180}$$

As in the SML analysis, incorporation of the $O(\epsilon)$ $f_1^{(\mathrm{U})}$ correction at the top of the RIR converts occurrences within these solutions of the RIR velocity scale U_l to the slowly varying incident velocity $U(z)$.

The outer region

Governing equations for the outer region are identical to (3.91)–(3.94). To reflect the displacement of the upper flow, it is convenient however to use $\exp \pm k(z-d)$ as the complementary functions of these equations rather than $\exp \pm kz$ as in the standard mixing length analysis. The leading order solutions are

$$w_o = C_o e^{-k(z-d)} + D_o e^{k(z-d)} + \int_{\tilde{z}}^{z} \frac{f(z') \cosh k(z-z')}{U(z')}\, dz'; \tag{3.181}$$

$$u_o = -iC_o e^{-k(z-d)} + iD_o e^{k(z-d)} + \frac{if}{kU} + i\int_{\tilde{z}}^{z} \frac{f(z') \sinh k(z-z')}{U(z')}\, dz'; \tag{3.182}$$

$$p_o = \frac{if}{k} - Uu_o. \tag{3.183}$$

Here D_o is determined by the condition of boundedness as $kz \to \infty$, namely

$$D_o + \frac{1}{2}\int_{\tilde{z}}^{\infty} \frac{f(z') e^{-k(z'-d)}}{U(z')}\, dz' = 0. \tag{3.184}$$

Matching the rooftop inner and outer regions

The $O(1)$ matching coordinate χ for the overlap region between the rooftop inner and outer regions is defined by

$$k(z-d) = \epsilon^{\alpha}\chi, \qquad \text{where} \quad 0 \le \alpha \le 1. \tag{3.185}$$

Matching the leading order vertical perturbation velocities in the overlap region gives

$$\tilde{w} = C_o + D_o; \tag{3.186}$$

the particular integrals over f match automatically. Matching the perturbation pressures gives

$$p_o = iU_l(C_o - D_o). \tag{3.187}$$

3.8.7 Matching the canopy region and upper flow analyses

The entire upper flow solution is linearly dependent on the velocity perturbations at the top of the canopy mixing region, $\tilde{u}$ and $\tilde{w}$, and therefore on s_1 and s_2. The values

of s_1 and s_2 are determined by requiring that the CMR and RIR pressures and shear stresses are continuous at $z = \tilde{z}$.

In practice it is easiest to do this by taking advantage of the linearity in s_1 and s_2. Calculate the discrepancies in pressure and shear stress when $s_1 = s_2 = 0$ ($\rightarrow \Delta p_{00}, \Delta\tau_{00}$), when $s_1 = 1, s_2 = 0$ ($\rightarrow \Delta p_{10}, \Delta\tau_{10}$) and when $s_1 = 0, s_2 = 1$ ($\rightarrow \Delta p_{01}, \Delta\tau_{01}$). Then the required values of s_1 and s_2 are given by

$$s_1 = \frac{(\Delta p_{01} - \Delta p_{00})\Delta\tau_{00} - (\Delta\tau_{01} - \Delta\tau_{00})\Delta p_{00}}{(\Delta\tau_{01} - \Delta\tau_{00})(\Delta p_{10} - \Delta p_{00}) - (\Delta p_{01} - \Delta p_{00})(\Delta\tau_{10} - \Delta\tau_{00})};$$

$$s_2 = \frac{(\Delta\tau_{10} - \Delta\tau_{00})\Delta p_{00} - (\Delta p_{10} - \Delta p_{00})\Delta\tau_{00}}{(\Delta\tau_{01} - \Delta\tau_{00})(\Delta p_{10} - \Delta p_{00}) - (\Delta p_{01} - \Delta p_{00})(\Delta\tau_{10} - \Delta\tau_{00})}.$$

3.8.8 Sample results

The displaced mixing length analysis introduces three new parameters that describe different aspects of the internal structure of a group of obstacles. These are λ, the constant mixing length within the canopy mixing region, $\tilde{z}$, the depth of the canopy mixing region, and z_o', the roughness height of the interface between the canopy mixing region and the linear mixing length flow above. In figures 3.18–3.20 we attempt to illustrate the impact each parameter has on the streamwise velocity perturbation by varying a single parameter in each figure. Thus figure 3.18 shows results obtained using a "central" parameter set, results with λ less than its central value, and results with λ greated than its central value; similarly figures 3.19 and 3.20 illustrate variation of z_o' and $\tilde{z}$ respectively. The values of all parameter sets are given in table 3.1. In addition, the dotted line in each figure shows the streamwise velocity perturbation predicted by the SML analysis. Figures 3.18–3.20 are calculated for the same force distribution and wavenumber as the small wavenumber SML sample results.

Variation of λ (figure 3.18)

As λ increases there is more efficient mixing over the depth of the canopy region. Hence velocity gradients are increasingly inhibited and the maximum velocity deficit is reduced. By continuity, the streamwise velocity deficit leads to a vertical velocity

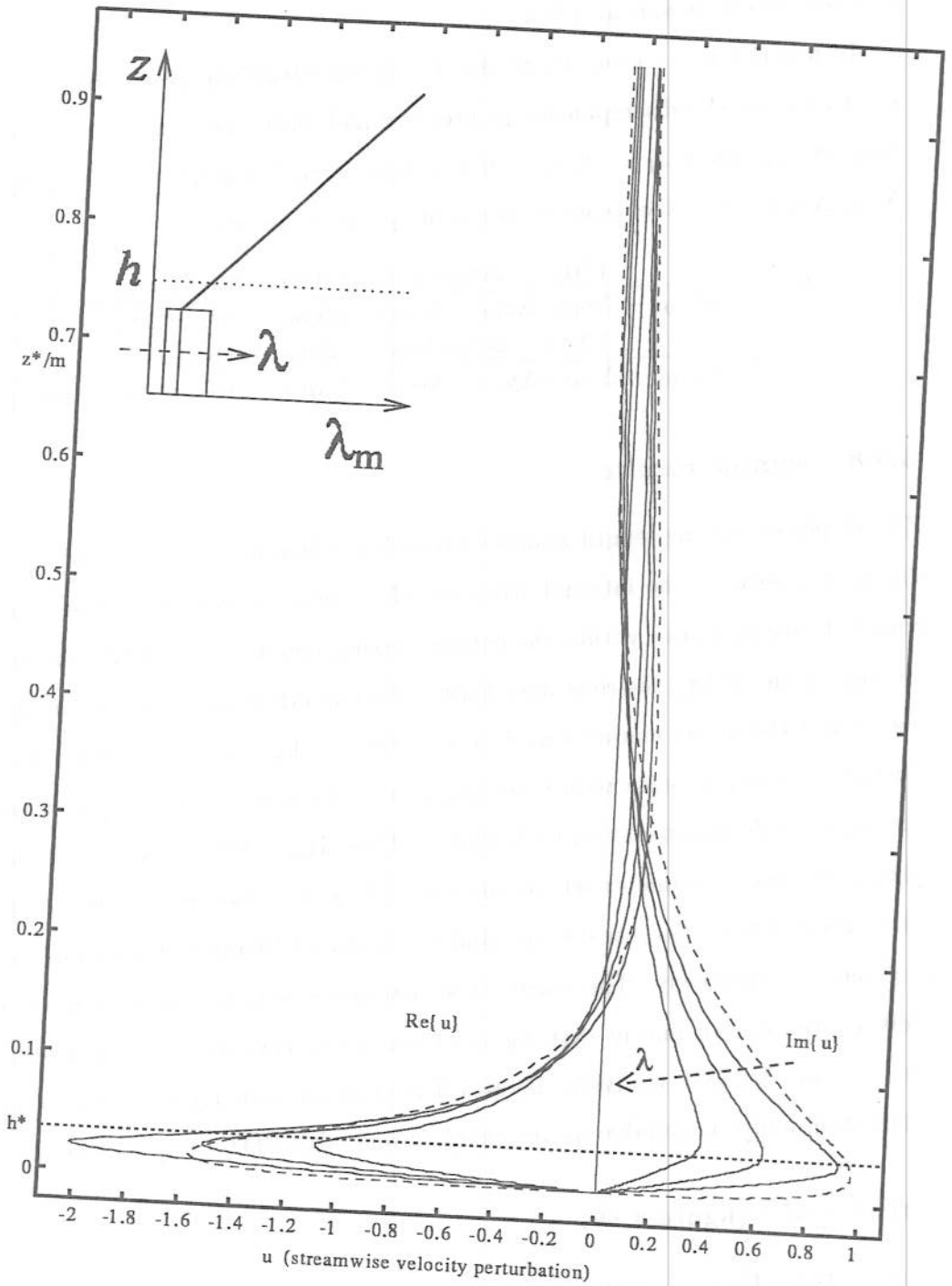

Figure 3.18: Variation of λ. The inset shows the mixing length profiles for each of the results graphed below. The dashed arrows indicate increasing λ.

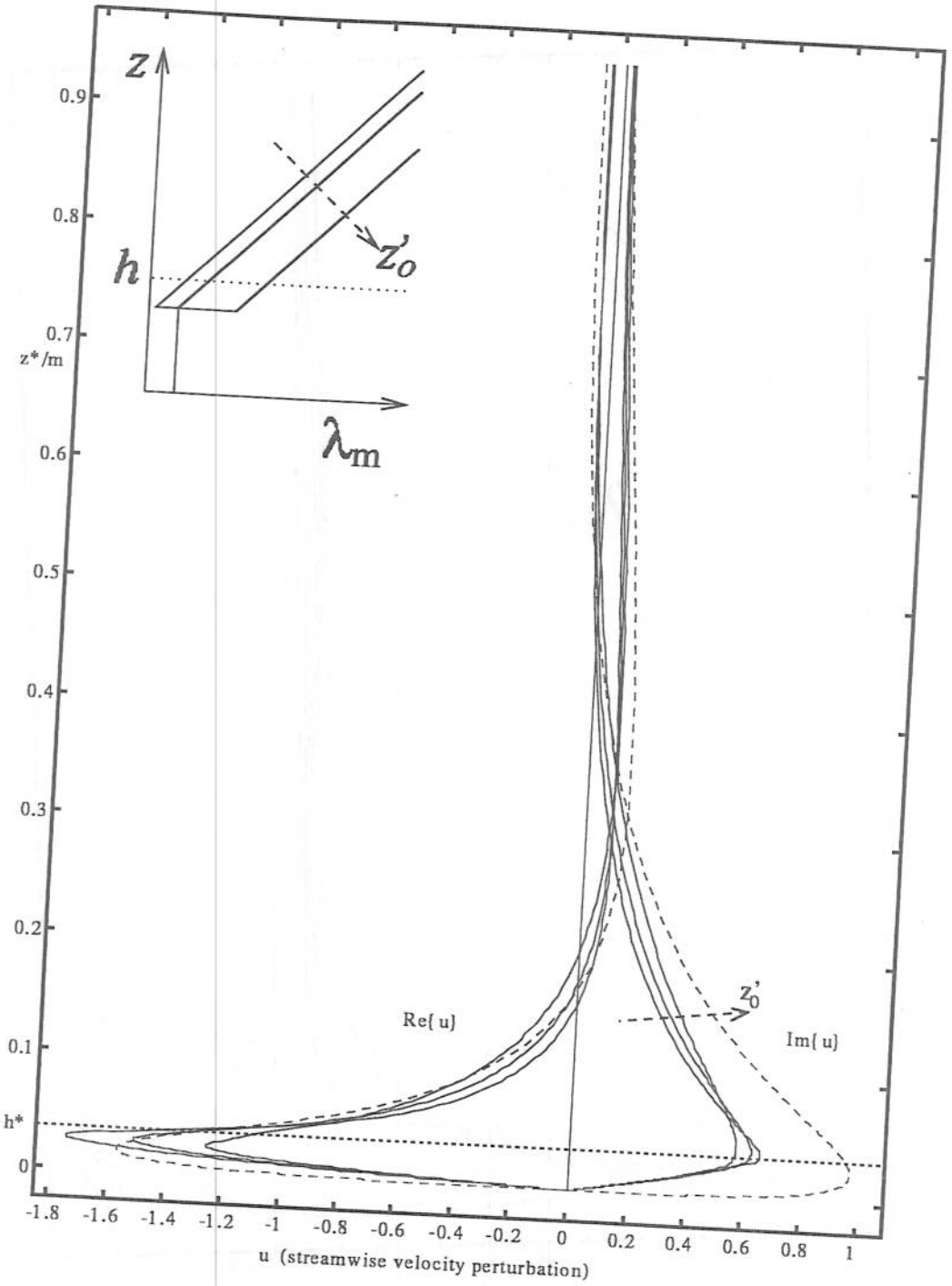

Figure 3.19: Variation of z_o'. The inset shows the mixing length profiles for each of the results graphed below. The dashed arrows indicate increasing z_o'.

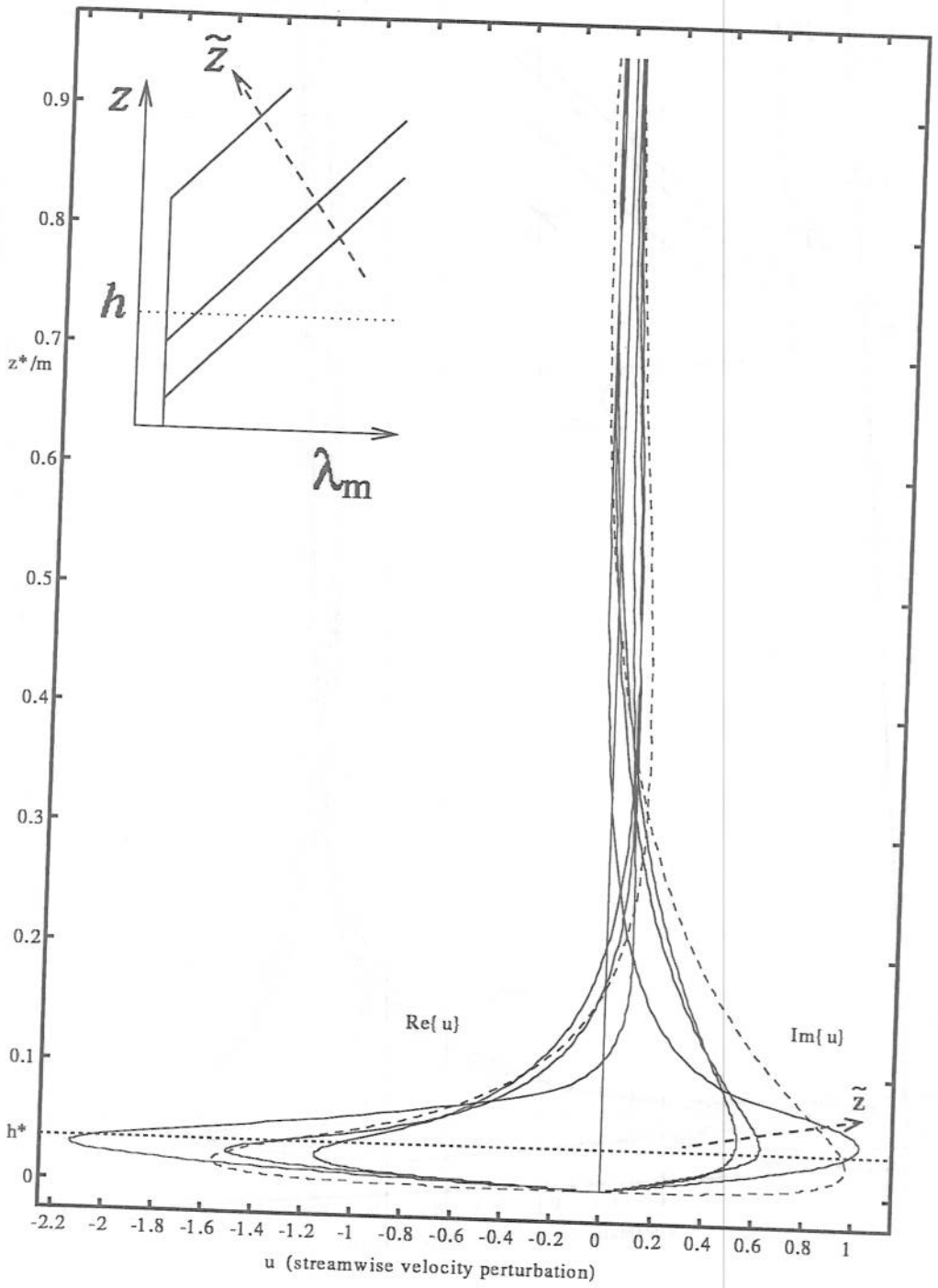

Figure 3.20: Variation of $\tilde{z}$. The inset shows the mixing length profiles for each of the results graphed below. The dashed arrows indicate increasing $\tilde{z}$.

	λ/h	z_o'/h	$\tilde{z}/h$	$\Rightarrow d/h$
Central parameter set	$\frac{1}{4}$	$\frac{1}{4}$	$\frac{3}{4}$	$\frac{1}{2}$
Reduced λ	$\frac{1}{8}$	$\frac{1}{4}$	$\frac{3}{4}$	$\frac{1}{2}$
Increased λ	$\frac{1}{2}$	$\frac{1}{4}$	$\frac{3}{4}$	$\frac{1}{2}$
Reduced z_o'	$\frac{1}{4}$	$\frac{1}{16}$	$\frac{3}{4}$	$\frac{11}{16}$
Increased z_o'	$\frac{1}{4}$	$\frac{3}{4}$	$\frac{3}{4}$	0
Reduced $\tilde{z}$	$\frac{1}{4}$	$\frac{1}{4}$	$\frac{1}{4}$	0
Increased $\tilde{z}$	$\frac{1}{4}$	$\frac{1}{4}$	2	$1\frac{3}{4}$

Table 3.1: The values of λ, z_o' and $\tilde{z}$ used in figures 3.18-3.20.

perturbation at the top of the canopy region, which in turn causes the speed up in streamwise velocity above the canopy. Since the parameters of the flow over this vertical perturbation velocity, z_o' and $d = \tilde{z} - z_o'$, are held constant, the speed up above the canopy increases or decreases with the velocity deficit within the canopy.

In the DML model the mixing length remains constant even very close to the ground where the blocking scale z must eventually dominate the canopy turbulence scale λ based on the dimensions of eddies shed from upstream obstacles. Thus significant velocity gradients that would be permitted near the ground by a mixing length of order z_o, the surface roughness, are inhibited by the constant DML model mixing length. This is a model weakness that could be compensated by reducing λ to a form $\propto z$ near the ground. Such a refinement is not attempted here because it might not be practical to make measurements that are consistent with the distributed force model so close to the ground.

Variation of z_o' (figure 3.19)

The interface roughness height or minimum mixing length in the shear layer, z_o', determines the gradients of streamwise velocity just above $z = \tilde{z}$: smaller z_o' gives larger

velocity gradients. Since speed up above the canopy is small compared with the maximum velocity deficit, the maximum velocity deficit is influenced by velocity gradients above $z = \tilde{z}$ and hence by z_o'. The canopy mixing region adjusts to meet this velocity deficit by changing its velocity perturbation only very close to $z = \tilde{z}$; cf. figure 3.18, in which variation of λ causes variation of velocity perturbation throughout the canopy mixing region.

Variation of $\tilde{z}$ (figure 3.20)

The inset graph shows how the mixing length starts increasing at $z = \tilde{z}$ from its minimum value in the canopy mixing region. Since $z_o' = \lambda$ for the cases shown in figure 3.20, $\tilde{z}$ determines the extent of the flow domain where the minimum mixing length applies. Increased $\tilde{z}$ means that stronger velocity gradients are allowed over more of the flow. The results with $\tilde{z}/h = 2$ show particularly strong gradients above the canopy; these are effectively laminar viscous results, since velocity variation above $z = 2h$ appears insensitive to the turbulence model.

3.9 Turbulence model sensitivity

Since the DML analysis of §3.8 includes the SML analysis as a special case ($z_o' = \tilde{z} = z_o$), the effects of varying the three DML parameters provide a good indication of the general sensitivity of the turbulent flow problem to changes in the turbulence closure model. On the one hand, the sample results exhibited in §3.8.8 show that dramatic changes in the streamwise velocity perturbation profile, *e.g.* up to 100% change in the maximum velocity deficit, can be effected by varying the DML parameters. On the other hand, they also show that such dramatic changes require extreme parameter values and that there is a large parameter space within which the theoretical predictions vary rather little. Even when extreme parameter values are used, the qualitative shapes of the perturbation quantity profiles remain similar in all cases.

In particular, the sample results show that the DML model with constant mixing

length in the force distribution can give very similar results to the SML model if the DML parameters are chosen appropriately (with the exception of the $z = O(z_o)$ layer near the ground where the SML model gives much stronger velocity gradients). This insensitivity of the turbulent analysis to the way the mixing length varies within the canopy is encouraging: it suggests that reservations over the use of a single length scale in the turbulence model are less relevant than originally expected.

The following chapter presents comparisons of the SML and DML results with experimental data and numerical simulations.